ARTICLE IN PRESS

Nature Communications

https://doi.org/10.1038/s41467-026-70580-3

Article in Press

A corticothalamic circuit modulates pain sensitivity and mediates innate fear-induced analgesia in male mice

Received: 16 March 2025

Accepted: 2 March 2026

Cite this article as: Jia, W.-B., Wang, X.-Y., Xia, X.-X. *et al.* A corticothalamic circuit modulates pain sensitivity and mediates innate fear-induced analgesia in male mice. *Nat Commun* (2026). https://doi.org/10.1038/s41467-026-70580-3

Wen-Bin Jia, Xin-Yue Wang, Xin-Xin Xia, Liu Tang, Yu-Xuan Liang, Xiao-Lin Lei, Xiao-Qing Liu, Wei Hu & Yan Zhang

We are providing an unedited version of this manuscript to give early access to its findings. Before final publication, the manuscript will undergo further editing. Please note there may be errors present which affect the content, and all legal disclaimers apply.

If this paper is publishing under a Transparent Peer Review model then Peer Review reports will publish with the final article.

ARTICLE IN PRESS

© The Author(s) 2026. **Open Access** This article is licensed under a Creative Commons Attribution-NonCommercial-NoDerivatives 4.0 International License, which permits any non-commercial use, sharing, distribution and reproduction in any medium or format, as long as you give appropriate credit to the original author(s) and the source, provide a link to the Creative Commons licence, and indicate if you modified the licensed material. You do not have permission under this licence to share adapted material derived from this article or parts of it. The images or other third party material in this article are included in the article's Creative Commons licence, unless indicated otherwise in a credit line to the material. If material is not included in the article's Creative Commons licence and your intended use is not permitted by statutory regulation or exceeds the permitted use, you will need to obtain permission directly from the copyright holder. To view a copy of this licence, visit http://creativecommons.org/licenses/by-nc-nd/4.0/.

ARTICLE IN PRESS

A corticothalamic circuit modulates pain sensitivity and mediates innate fear-induced analgesia in male mice

Wen-Bin Jia[1*], Xin-Yue Wang[1*], Xin-Xin Xia[1*], Liu Tang[1*], Yu-Xuan Liang[1], Xiao-Lin Lei,[1] Xiao-Qing Liu,[2] Wei Hu[1 †] and Yan Zhang[1†]

[1]Department of Neurology, Centre for Leading Medicine and Advanced Technologies of IHM, The First Affiliated Hospital of USTC, Division of Life Sciences and Medicine, University of Science and Technology of China, Hefei 230001, China

[2]School of Basic Medical Sciences, Division of Life Sciences and Medicine, University of Science and Technology of China, 230027 Hefei, China

[*]These authors contributed equally

[†]Correspondence to:

Yan Zhang, E-mail: yzhang19@ustc.edu.cn (Y.Z.)

Wei Hu, E-mail: andinghu@ustc.edu.cn (W.H.)

ARTICLE IN PRESS

ARTICLE IN PRESS

Abstract

Fear and pain are two frequently co-occurring states that mammals need to orchestrate to ensure survival. Nevertheless, how the brain dynamically prioritizes between them remains poorly understood. Here, we demonstrate that innate fear suppresses both acute and chronic pain, whereas pain does not reciprocally modulate fear responses in male mice. Using fiber photometry, virus tracing, and electrophysiological approaches, we show that exposure to a fear-inducing odor activates GABAergic neurons in the anterior piriform cortex (APC), which subsequently attenuates pain-associated hyperactivity in the downstream mediodorsal thalamus (MD). Crucially, inhibiting either APC^{GABA} neurons or the APC^{GABA}-MD circuit enhances pain sensitivity and abolishes fear-induced analgesia. Conversely, activation of APC^{GABA} neurons or the APC^{GABA}-MD circuit induces freezing responses and relieves pain, mimicking fear-induced analgesia. These findings unveil a corticothalamic circuit that bidirectionally regulates pain processing and underlies fear-provoked analgesia, offering potential therapeutic avenues for pain management.

Introduction

When facing dynamic physiological and environmental challenges, mammals must rapidly prioritize survival-critical needs to execute appropriate adaptive behaviors[1-3]. While significant progress has been made in understanding how the central nervous system processes individual states such as fear[4], pain[5,6], hunger[5], and thirst[6], the mechanisms by which the brain hierarchically organizes competing survival demands remain poorly understood.

Previous research has reported interactions between pain and other conflicting states such as hunger, thirst, caloric deprivation or acute stressors[5-9]. In such conflicts, behavioral priorities typically shift from nocifensive response – defined as an organism's defensive response to potentially harmful stimuli, typically involving pain perception and avoidance movements – toward addressing more immediate survival needs[5,7-10]. Fear, as a fundamental emotion arising from threat, is a frequently encountered state. While conditioned fear-induced analgesia and its neural substrates have been extensively characterized[4,11-13], innate fear responses—particularly those elicited by natural predators—remain comparatively unexplored despite their ecological

ARTICLE IN PRESS

relevance. For most species, predators serve as the primary threat sources. In such cases, survival demands immediate fight-or-flight decisions, requiring temporary suppression of pain processing to facilitate predator confrontation or evasion[9,14,15]. Surprisingly, little is known to date about the neural mechanisms underlying how the brain makes preferential choices between the intractable conditions of innate fear and pain. In this study, we utilized the odorant molecule of 2-methyl-2-thiazoline (2MT), chemically related to the fox anogenital gland secretion 2,4,5-trimethyl3-thiazoline (TMT), to induce an innate fear state in mice[16]. Therefore, our study focused on the olfactory system to elucidate ranking mechanisms of innate fear and pain processing.

The piriform cortex (PC) serves as the primary olfactory cortex, receiving odorant information inputs from the upstream olfactory bulb (OB) and lateral olfactory tract (LOT) regions[17]. This region plays integral roles in olfactory information processing[18,19], learning[20], memory[21,22], and has been implicated in innate fear responses[23,24]. Anatomically, the PC is subdivided into anterior (APC) and posterior (PPC) regions[25].

Here, we demonstrate that innate fear endogenously inhibits pain, whereas pain does not affect fear reactions. We further identify the APC as a node in innate fear-induced analgesia, mediated specifically by a GABAergic projection to the mediodorsal thalamus (MD). Notably, the constitutive activity of both APC^{GABA} neurons and the APC^{GABA}-MD circuit exerts tonic gating of pain perception. Taken together, our findings reveal an olfactory-embedded corticothalamic circuit that bidirectionally modulates pain processing and mediates fear-induced analgesia, while shedding light on potential therapeutic targets for pain management.

Results

Innate fear odor 2MT induces analgesia in mice

To investigate whether innate fear affects both acute and chronic pain, a potent predator-derived odor compound of 2MT which evokes freezing response, a behavioral readout of fear[16,26,27], was exposure to mice. Anisole, a neutral odor, served as a control to rule out non-specific responses to olfactory stimulation (Supplementary Fig. 1). Separate cohorts of mice were then subjected to a series of pain sensitivity tests, as described below. We first examined mechanical and thermal

ARTICLE IN PRESS

sensitivity by von Frey filaments and radiant heat, respectively. Upon 2MT exposure in naïve mice, we observed a remarkable elevation of the paw withdrawal threshold and paw withdrawal latency compared to both water and anisole controls (Fig. 1a), indicating a reduction in basal nociception. By contrast, the pain sensitivity of anisole-exposed mice was unchanged (Fig. 1a).

Next, hot plate and pinprick assays were used to assess acute thermal pain and mechanical pain, respectively. In the hot plate test, exposure to 2MT significantly prolonged the latencies to both jumping and licking and reduced the episodes of these behaviors compared to the water treatment, whereas anisole had no significant effect (Fig. 1b). In the subsequent studies, the two nociceptive behaviors were analyzed as a combined measure. Innate fear odor induced by 2MT also significantly reduced the response frequency to noxious mechanical (pinprick) stimulation of the hind paw (Fig. 1c). Together with the hot plate test results, these findings demonstrate that innate fear odor profoundly alleviates both forms of acute pain.

Finally, we explored 2MT-induced analgesia in models of pathological pain. We found that 2MT, but not a neutral odor, markedly alleviated pain behaviors across multiple models: the nociceptive licking responses in acute inflammatory pain model (Formalin), as well as tactile and thermal hypersensitivity in both complete Freund's adjuvant (CFA)-induced inflammation and spared nerve injury (SNI)-induced neuropathic pain models (Fig. 1d-f).

Since the key behavior readouts of pain sensitivity tests (e.g., increased thresholds, reduced nocifensive responses) rely on motor performance, we investigate whether 2MT exposure could produce motor suppression that might confound the interpretation of analgesic effects. First, the grip strength test was used to evaluate muscle force. We observed no significant difference in grip strength between 2MT-exposed mice and water-exposed controls (Supplementary Fig. 2a). Additionally, high-speed paw kinematics analysis during the pinprick assay revealed comparable paw withdrawal velocity and amplitudes between the two groups (Supplementary Fig. 2b), indicating normal motor output. To further assess motor function, we evaluated motor coordination and balance using the balance beam and rotarod tests. No differences were detected in traversal time (balance beam) or latency-to-fall (rotarod) between 2MT- and water-treated mice

ARTICLE IN PRESS

(Supplementary Fig. 2c, d). Our results show no differences in traversal time and consistent latency-to-fall between 2MT- and water-exposed mice. These results demonstrate that the observed analgesic effects of 2MT are not attributable to motor impairment.

Altogether, our data demonstrate that an innate fear state can reliably provoke analgesia in both physiological and pathological conditions.

APC^{GABA} neurons respond to innate fear odor 2MT

The piriform cortex (PC) has long been thought to encode olfactory information and odor fear memory[18,22]. Therefore, we hypothesized that PC neurons might also mediate 2MT-induced analgesia. To test this, we employed *TRAP2::Ai14* mice to selectively label neurons activated during 2MT exposure. We found that 2MT exposure paired with the injection of 4-Hydroxytamoxifen (4-OHT) results in substantial expression of tdTomato in the PC. Quantitative analysis showed that the fold change of 2MT-TRAPed tdTomato-positive neurons relative to the water control was significantly greater in the APC than in the PPC (Fig. 2a, b). Based on this pronounced activation, we therefore focused subsequent investigations on the role of the APC in fear-induced analgesia.

To validate whether the Fos-TRAP line works as previously[28], we re-exposed 2MT-TRAPed *TRAP2::Ai14* mice to either 2MT or anisole. c-Fos immunostaining indicated that approximately 64% of 2MT-TRAPed APC neurons were reactivated by 2MT, compared to only ~23% upon anisole re-exposure (Supplementary Fig. 3), confirming the system's efficacy for activity-dependent labeling.

Next, we employed in vivo fiber photometry to record the real-time population activity of APC neurons in response to 2MT. Following injection of AAV-hSyn-GCaMP6m into the unilateral APC and optical fiber implantation above the injection site (Supplementary Fig. 4a, b), we observed a rapid and robust increase in calcium signal upon 2MT presentation via air puff or cotton swab. In contrast, water or anisole exposure evoked only mild calcium transients (Supplementary Fig. 4c, d). These findings provide additional evidence for APC neurons in processing fear-related olfactory information.

ARTICLE IN PRESS

The piriform cortex comprises heterogeneous populations of excitatory and inhibitory neurons. To dissect the specific cell types within the APC mediating fear-induced analgesia, we performed fluorescence in situ hybridization (FISH) to determine whether the 2MT-TRAPed neurons were GABAergic (GAD2-positive) or glutamatergic (CAMKII-positive). Interestingly, upon 2MT exposure, the proportion of $GAD2^+$ cells among the tdTomato-labeled neurons significantly increased compared to the control groups. In contrast, the proportion of $CaMKII^+$ cells remained unchanged (Fig. 2c, d). These data indicate that the fear odor 2MT recruits a larger fraction of APC^{GABA} neurons than does a neutral odor, while APC^{GLU} neurons are equally recruited by both odor types.

To further characterize odor-evoked activation patterns in distinct neuronal populations, we performed in vivo fiber photometry recordings of both inhibitory neurons and excitatory neurons in the APC. We first targeted inhibitory neurons by injecting AAV-DIO-GCaMP6m into the APC of *VGAT-Cre* mice (Fig. 2e, left). Virus expression and fiber placement were verified upon completion of behavioral tests (Fig. 2e, right). Odor stimuli were delivered via either air puff or cotton swab (Fig. 2f). Each odor was tested across six repeated trials with 1-minute inter-trial intervals. Consistent with our FISH data, fiber photometry revealed a striking difference in odor response profiles. The fear odor 2MT elicited larger calcium transients in inhibitory neurons compared to water exposure, while anisole exposure resulted in only mild changes in calcium signals relative to water controls (Fig. 2g, h). In marked contrast, recordings from excitatory neurons of *CAMKII-Cre* mice showed that 2MT and anisole exposure elicited calcium transients to a similar extent when compared to water exposure (Fig. 2i-l). Successive odor exposure can cause odorant adaptation in the olfactory receptor cell[29], which might in turn affect APC neural activity. However, our trial-by-trial analysis demonstrated stable calcium response magnitudes across six trials of anisole or 2MT exposure (Supplementary Fig. 5). This consistency confirms that the 1-minute inter-trial interval effectively prevents olfactory adaptation.

We further validated these cell-type-specific response patterns in *C57* mice through viral-mediated expression of GCaMP6s under either VGAT or CaMKII promoters. Consistent with

ARTICLE IN PRESS

above Cre-line observations, this population-specific activation dichotomy was observed (Supplementary Fig. 4e-l).

Our findings provide evidence that APC^{GABA} neurons selectively response to the fear odor 2MT.

APC^{GABA} neurons mediate 2MT-induced analgesia

Given that APC^{GABA} neurons exhibit selective tuning to innate fear odor, we hypothesized that these neurons play a crucial role in fear analgesia. To further investigate this, we conducted a series of pain-related tests sequentially in the same cohort of mice following the transient silencing of APC^{GABA} neurons, ranging from mild pain-inducing stimuli (assessing basal nociception) to nerve injury operation. To achieve this, an adeno-associated virus (AAV) carrying the inhibitory hM4Di receptor under the control of the GABAergic neuron promoter (AAV-VGAT-hM4D(Gi)-mCherry) or an AAV-VGAT-mCherry as a control was injected into the bilateral APC of *C57* mice. The specificity of the VGAT-promoter driven viruses was further verified in *VGAT-Cre* mice, which received simultaneous injections of AAV-DIO-EYFP and AAV-VGAT-mCherry into the APC (Supplementary Fig. 6a). We found that approximately 72% of mCherry-positive neurons were also EYFP-positive (Supplementary Fig. 6b, c). Twenty-one days after viral injection, mice received an intraperitoneally (i.p.) injection of clozapine-N-oxide (CNO). Subsequently, the mice were exposed to 2MT and then underwent behavioral testing (Fig. 3a). Post hoc staining showed that the majority of mCherry-expressing neurons were GABA-positive, confirming high specificity of viral targeting (Fig. 3b). Electrophysiological recordings validated the efficacy of the chemogenetic approach, showing that CNO hyperpolarized the resting membrane potential (RMP) and blocked action potential firing in hM4Di-expressing neurons (Fig. 3c). Considering that our behavioral assays necessitate a two-day protocol, we examined whether repeated 2MT exposure affects pain responses. To this end, we analyzed 2MT-induced analgesia on basal nociception from *C57* mice over two consecutive days. We did not detect any differences in both mechanical and thermal pain threshold (Supplementary Fig. 7), proving that repeated 2MT exposure across two days does not affect the degree of fear analgesia. Therefore, subsequent behavioral experiments followed a two-day schedule: intraperitoneal saline administration on the first day, followed by

ARTICLE IN PRESS

CNO on the second day. Notably, chemogenetic inhibition of APC^{GABA} neurons did not affect 2MT-induced freezing behavior, regardless of the saline and CNO treatment order (Supplementary Fig. 8a-c), but significantly attenuated the protective effects of fear on basal nociception, acute thermal pain and chronic neuropathic pain (Fig. 3d-f). Importantly, inhibition of APC^{GABA} neurons did not impair motor performance, as confirmed by grip strength, high-speed paw kinematics, balance beam, rotarod, and OFT assessments (Supplementary Fig. 9a-f), suggesting that changes in the above pain-related tests were not due to motor performance deficit.

Repeated pain testing in the same mice across multiple conditions could alter subsequent sensitivity, introducing possible confounds. To mitigate potential order effects, we implemented a counterbalanced experimental design for the sequence of pain sensitivity tests. In naïve *C57* mice, we counterbalanced four test modalities (von Frey, Hargreaves', hot plate and pinprick tests; Supplementary Fig. 10a), while in nerve-injured and CFA-injected mice, we counterbalanced two sets of pain test (von Frey and Hargreaves' tests, Supplementary Fig. 10f). We found that baseline sensitivity of all behavioral assays remained stable, independent of testing order. Importantly, the sequence of testing did not affect the magnitude of 2MT-induced analgesia (Supplementary Fig. 10b-e, g, h). Based on these findings, we maintained the same sequential pain testing protocol as used in above chemogenetic inhibition for subsequent neural manipulation experiments.

In our study, we also included a battery of pain sensitivity tests without 2MT exposure but having APC^{GABA} neural inhibition in naïve mice (Supplementary Fig. 11a). Interestingly, silencing APC^{GABA} neurons resulted in both mechanical and thermal hypersensitivity (Supplementary Fig. 11b). Since pain involves more than nocifensive responses, we also assessed its affective component using conditioned place aversion (CPA)[30]. We found that silencing APC^{GABA} neuron alone produced significant CPA (Supplementary Fig. 11c). These data indicate that the constitutive activity of APC^{GABA} neurons modulates both pain sensation and its associated negative affect.

Due to the hypersensitivity after the silencing of APC^{GABA} neurons, the observed loss of fear analgesia may stem from alterations in baseline pain sensitivity. Furthermore, approximately ~40% of APC^{GABA} neurons were activated by 2MT (Supplementary Fig. 12a-c), manipulating broad

ARTICLE IN PRESS

APC^{GABA} population could confound the interpretation of results. To specifically dissociate the role of the fear odor-responsive neuronal ensemble from general nociceptive processing, we employed a TRAP2 strategy to selectively target 2MT-activated APC inhibitory neurons. We bilaterally injected either AAV-VGAT-DIO-hM4Di-mCherry or AAV-VGAT-DIO-mCherry into the APC of TRAP2 mice, followed by 2MT exposure paired with 4-OHT injection (Fig. 4a). This approach allowed for the specific chemogenetic inhibition of neurons recruited by the innate fear odor. The virus expression and spillover was verified across included hM4Di-injected mice (Fig. 4b). We found that inhibiting this ensemble attenuated 2MT-induced fear expression (Fig. 4c). Strikingly, although it did not change baseline thermal or mechanical nociception, it significantly attenuated 2MT-induced analgesia (Fig. 4d, e), with no effect on locomotion (Fig. 4g-k). These findings establish a necessary role for 2MT-responsive APC^{GABA} neurons in mediating innate fear-induced analgesia and demonstrate their functional segregation from basal nociceptive processing.

To gain further insight into the contribution of APC^{GABA} neurons to fear analgesia, we explored behavioral consequences of activating these neurons. To this end, we administered an adeno-associated virus (AAV) carrying the excitatory hM3Dq receptor under the control of the VGAT promoter (AAV-VGAT-hM3D(Gq)-mCherry) into the APC region of *C57* mice (Fig. 3g). CNO-induced membrane depolarization and neural firing in hM3Dq-expressing neurons verified viral functionality (Fig. 3h). Intriguingly, activation of APC^{GABA} neurons exhibited a resemblance to the behavioral phenotypes observed in the innate fear context. There was a significant increase in freezing response and a decrease in total distance traveled in the 20-minute session (Supplementary Fig. 8d, e). Importantly, both mechanical and thermal nociception were significantly decreased (Fig. 3i). There was also a significant reduction in nocifensive responses towards noxious thermal stimulation in naïve mice (Fig. 3j). Of note, a prominent analgesia in nerve-injured mice was observed (Fig. 3k). To investigate whether activating APC^{GABA} neurons induces pain-relief-seeking behavior, we performed a classic conditional place preference (CPP) test in SNI mice. Indeed, hM3Dq-injected SNI mice displayed a significant greater chamber preference score for the CNO-paired context than did mCherry-injected controls (Fig. 3l). Furthermore, gross or fine

ARTICLE IN PRESS

motor control, assessed by grip strength, high-speed paw kinematics, balance beam, rotarod tests, along with the total distance traveled in a 5-minute OFT remained unchanged following chemogenetic activation of APC^{GABA} neurons (Supplementary Fig. 9g-k). These results suggest that APC^{GABA} neuron activity is sufficient to produce both fear-like behaviors and analgesia.

Following 2MT exposure (Supplementary Fig. 11d), we assessed pain sensitivity and found that exciting APC^{GABA} neurons further enhanced the fear analgesia. Specifically, this enhancement was observed on mechanical nociception under normal conditions, and on both mechanical allodynia and thermal hypersensitivity in neuropathic pain conditions. However, no further reduction was seen in baseline thermal nociception and acute thermal pain responses (Supplementary Fig. 11e, f), likely due to a ceiling effect from maximal 2MT-induced analgesia.

To complement our inhibition studies, we also employed the TRAP2 strategy to selectively activate 2MT-responsive APC inhibitory neurons (Fig. 4l, m). This manipulation was sufficient to induce both freezing behavior and produce significant analgesia (Fig. 4n-p), again without affecting locomotion assessed by grip strength, high-speed paw kinematics, balance beam and rotarod (Fig. 4q-t). The observed decrease in total distance traveled in the OFT is consistent with the induction of freezing behavior following neural activation (Fig. 4u). These complementary loss- and gain-of-function results collectively demonstrate that 2MT-responsive APC^{GABA} neurons are both necessary and sufficient in mediating innate fear-related analgesia.

Taken together, our data define a critical role for APC^{GABA} neurons in mediating fear-induced analgesia, in addition to their constitutive regulation of basal pain perception.

MD is likely APC's target to mediate 2MT-induced analgesia in chronic neuropathic pain

To investigate the downstream target of APC^{GABA} neurons that mediate fear-induced analgesia, we conducted anterograde tracing. We injected an AAV-VGAT-mCherry into the unilateral APC of *C57* mice to visualize axon projections (Fig. 5a). Given the APC's location on the ventrolateral cortical surface, near several pain-related regions—including the lateral nucleus accumbens (LatNAc)[31,32], ventral pallidum (VP)[33], anterior insular cortex (AIC)[34], and reticular thalamic nucleus (TRN)[35], which are associated with pain and some of which project to the MD[35,36], we

ARTICLE IN PRESS

carefully assessed potential viral spread beyond the APC. Analysis confirmed minimal to no spillover to AIC and TRN (Supplementary Fig. 13). Next, we mapped the projection targets of APC^{GABA} neurons, observing dense neural fibers in the mediodorsal thalamus (MD), ventral lateral nucleus of the thalamus (VL), and substantia nigra pars reticulata (SNR) (Fig. 5b). To validate the functional connectivity of these projections, we injected AAV-VGAT-ChR2 into the APC. After two weeks for expression, we performed whole-cell patch clamp recordings in brain slices containing the MD, VL, or SNR. Blue light stimulation reliably elicited inhibitory postsynaptic currents (IPSCs) in neurons within each of these regions. These IPSCs were abolished by bath application of bicuculline (10 μM), an antagonist of $GABA_A$ receptors (Fig. 5c), confirming that these projections are GABAergic.

To identify which projection targets of APC^{GABA} neurons mediate fear analgesia, we systematically compared neuronal excitability in each target region. We conducted whole-cell patch clamp recordings from neuropathic (SNI) and sham-control mice. In the MD of SNI mice, we found a significantly increased firing rate and a depolarized membrane potentials (RMP) compared to sham controls (Fig. 4d), indicating enhanced neuronal excitability following nerve injury. In contrast, the excitability of neurons in the VL and SNR remained unchanged (Fig. 4d).

We next investigated whether innate fear could reverse the SNI-induced hyperexcitability of MD neurons. Remarkably, 2MT exposure effectively normalized these pathological changes (Fig. 5e-g), as evidenced by the rescue of firing rate, resting membrane potential, and rheobase. This functional recovery implies a key role for the MD in the interplay between innate fear and neuropathic pain. In addition, 2MT exposure significantly reduced the input resistance (R_{in}) of MD neurons (Fig. 5h), a change indicative of increased spontaneous inhibitory input. Consistent with this, recordings of spontaneous inhibitory postsynaptic currents (sIPSCs) in MD neurons in SNI mice revealed that 2MT treatment 2MT significantly increased sIPSC frequency without affecting amplitude (Fig. 5i), indicating a presynaptic enhancement of inhibitory transmission onto MD neurons.

Collectively, these findings provide a plausible mechanism by which 2MT exposure strengthens

ARTICLE IN PRESS

APC^{GABA}→MD inhibition, leading to persistent normalization of MD excitability and alleviation of neuropathic pain.

We further confirmed the monosynaptic nature of APC^{GABA}-MD connection. Light-evoked responses were completely blocked by tetrodotoxin (TTX) and partially restored upon application of 4-aminopyridine (4-AP), a potassium channel blocker (Fig. 5j). The recovered responses were subsequently blocked by bicuculline, confirming a direct, monosynaptic GABAergic pathway.

Inhibition of MD-projecting APC^{GABA} neurons dampens fear impact on pain and SNI-induced neural dysfunction

If the APC^{GABA}-MD pathway plays an essential role in fear analgesia, then inhibition of MD-upstream PC^{GABA} neurons may dampen this effect. To test this hypothesis, we injected AAV2/2-retro-hSyn-Cre into the MD and AAV-VGAT-DIO-hM4D(Gi)-mCherry (or control AAV-VGAT-DIO-mCherry) into the APC of *C57* mice. Three weeks later, CNO was administrated intraperitoneally to inhibit MD-upstream APC^{GABA} neurons during 2MT presentation, followed by the same battery of pain tests as described previously (Fig. 6a). Post hoc staining showed that approximately 81% of mCherry-expressing APC neurons were GABA-positive, indicating specific targeting of MD-upstream GABAergic neurons (Fig. 6b). Furthermore, CNO-induced membrane hyperpolarization of hM4Di-expressing APC^{GABA} neurons verified functional inhibition (Fig. 6c). As predicted, chemogenetic inhibition of MD-projecting APC^{GABA} neurons significantly reduced 2MT-induced analgesia across multiple pain modalities, including basal nociception, acute thermal pain, and chronic neuropathic pain (Fig. 6d-f). Of note, this manipulation did not affect fear odor-induced freezing behavior, regardless of the saline and CNO treatment order (Supplementary Fig. 8f-h). Importantly, this loss of analgesia was not due to motor impairment, as evidenced by a comprehensive suits of behavioral assays including grip strength, paw kinematics, balance beam, rotarod and open field tests (Supplementary Fig. 9k-o).

To further define the role of MD-projecting APC^{GABA} neurons in innate fear-induced analgesia, we quantified their activation by the fear odorant 2MT. Our data revealed that approximately 78% of MD-projecting APC^{GABA} neurons were activated by 2MT (Supplementary Fig. 12d-f). This

ARTICLE IN PRESS

indicates that the vast majority of APC GABAergic cells are activated by fear odorant.

Given that inhibition of MD-upstream APC^{GABA} neurons dramatically attenuated 2MT-induced analgesia under neuropathic pain conditions (Fig. 6f), we next investigated whether this manipulation would prevent the rescue of MD hyperexcitability by 2MT in the chronic pain state. To address this, we performed patch clamp recordings from MD neurons in SNI mice expressing either mCherry or hM4Di in MD-upstream APC^{GABA} neurons. These mice received intraperitoneal CNO injections (30 minutes prior) to either 1-hour 2MT exposure or water exposure. Acute brain slices containing the MD thalamus were then prepared for electrophysiological recordings. In the absence of 2MT, inhibition of MD-projecting APC^{GABA} neurons did not alter SNI-induced MD hyperactivity assessed by firing rate and rheobase, compared with mCherry controls (Fig. 6g-i). This was likely due to a ceiling effect from maximal SNI-induced MD neural hyperactivity. In contrast, while 2MT exposure effectively rescued MD hyperactivity in control (mCherry-expressing) mice, this therapeutic effect was completely abolished in inhibitory hM4Di expressing mice (Fig. 6g-h). This lack of response to 2MT in chemogenetically silenced mice suggests that functional APC-MD GABAergic transmission is essential for reversing SNI-induced MD hyperactivity.

These data collectively reveal that MD-upstream APC^{GABA} neurons critically regulate fear impact on pain and nerve injury-induced MD neural dysfunction**.**

To investigate the physiological role of MD-projecting APC^{GABA} neurons, we inhibited them in naïve mice without 2MT exposure (Supplementary Fig. 14a). This inhibition induced both mechanical and thermal hypersensitivity (Supplementary Fig. 14b) and established an aversive state, as measured by conditioned place aversion (CPA) (Supplementary Fig. 14c). These results demonstrate that this pathway exerts a tonic inhibitory control over basal pain perception, in addition to its critical role in mediating fear-induced analgesia.

The APC^{GABA}-MD circuit mediates 2MT-induced analgesia.

To deepen our understanding of how the APC^{GABA}-MD circuit mediates fear analgesia, we first tested the necessity of APC^{GABA}-MD projections in fear-induced analgesia. We thus injected AAV-

ARTICLE IN PRESS

VGAT-eNpHR-EYFP into the APC region and implanted optic fibers bilaterally over the MD, enabling a circuit-specific inhibition in freely moving mice. AAV-VGAT-EYFP was injected as the control (Fig. 7a). The accuracy of optic fiber placement was validated (Fig. 7b). Electrophysiological recordings from the eNpHR-EYFP^{+} APC neurons across multiple mice confirmed the viability of functional virus expression (Fig. 7c). We showed that optogenetic inhibition of APC^{GABA} terminals within the MD greatly diminished the analgesic effects of 2MT, both in naïve mice and those with SNI (Fig. 7d-f).

Without the 2MT exposure, optogenetic inhibition of the MD-projecting APC^{GABA} terminals in naïve mice resulted in hypersensitivity and the formation of aversive memory (Supplementary Fig. 15a-c), as observed in mice when the APC^{GABA} neurons were chemogenetically inhibited (Supplementary Fig. 11a-c).

Next, we conducted experiments to assess the sufficiency of APC^{GABA}-MD circuit activity in fear analgesia. To this end, AAV-VGAT-ChR2-mCherry or AAV-VGAT-mCherry was injected into the APC and optic fibers were bilaterally implanted over the MD (Fig. 7g). Current clamp recordings on ChR2 -mCherry^{+}-expressing APC neurons showed that blue light stimulation (20 Hz) reliably evoked neural firing across multiple neurons (Fig. 7h). As expected, optogenetic activation of APC^{GABA} terminals within the MD was sufficient to produce analgesia in various pain tests (Fig. 7i-k), phenocopied the behavioral pattern in the innate fear context (Fig. 1) or the effects of APC^{GABA} neural activation (Fig. 3i-k). Furthermore, we observed a striking dissociation in conditioned place preference: SNI mice showed a significant preference for the chamber paired with optogenetic activation of APC^{GABA} neuron terminals in the MD (Fig. 7l), whereas naïve mice displayed no such preference (Supplementary Fig. 16). This pain-context-specific behavioral reinforcement establishes that the rewarding effect is contingent upon the relief of neuropathic pain, rather than a general rewarding effect.

In the pain test with 2MT exposure, APC^{GABA}-MD circuit activation further enhanced the fear-evoked analgesia on chronic neuropathic pain (Supplementary Fig. 16d-g).

Collectively, we present compelling evidence demonstrating that the APC^{GABA}-MD circuit

ARTICLE IN PRESS

mediates innate fear-induced analgesia and regulates pain perception.

The innate fear responses are not affected by pain.

To ensure survival, mammals need to cope with the most critical threats. We then examined how the pain affects innate fear behavior. We observed that prior exposure to a 47℃ hot plate or 10 min-pinprick stimuli pinprick has no influence on the fear reaction assessed by the proportion of freezing time, movement distance, odor zone entries, and time in the odor zone during innate fear contexts (Fig. 8a-d). Mice experiencing inflammatory pain or neuropathic pain also exhibited similar levels of 2MT-induced fear reaction when compared to their respective control groups (Fig. 8e-h). These findings suggest that the innate fear is not affected by pain.

Discussion

Survival in dynamic environments requires mammals to rapidly adapt and respond to critical challenges. Addressing immediate threats is essential for enhancing survival probability. Here, we demonstrate that mice prioritize innate fear responses over pain perception and identify a neural circuit from the APC to MD that is both necessary and sufficient for mediating innate fear-evoked analgesia (Supplementary Fig 17).

Upon threat detection, the brain orchestrates a suite of physiological and psychological reactions termed the fear response[37]. This state is accompanied by modified pain processing, ensuring that the animal's attention is not distracted. While learned fear-conditioned analgesia has been extensively studied for over five decades, with well-established mechanisms involving amygdala activation[38-40], and subsequent engagement of descending pain modulatory pathways (e.g., periaqueductal gray and rostral ventromedial medulla), the neural substrates underlying unconditioned fear-induced analgesia remain less explored. Our study systematically assessed multiple types of physiological and pathological pain under predator odor 2MT. Notably, beyond replicating the alleviation of physiological pain and previously reported formalin-induced inflammatory pain[9,41], we observed robust analgesic effects in both chronic neuropathic and persistent inflammatory pain models.

ARTICLE IN PRESS

Chronic pain affects approximately 20% of the human population[42] and is recognized as a maladaptive condition involving central mechanisms[43-47]. Among its various forms, neuropathic pain represents one of the most refractory conditions encountered in clinical practice. Understanding the brain's intrinsic modulatory mechanisms may therefore facilitate the development of more effective therapeutic strategies. Non-pharmacological, noninvasive approaches to chronic pain management – including sensory stimulation through music, green light exposure, and odorant molecules such as linalool – have long been reported[48-50]. The visual and auditory cortex-based neural substrates for light and music therapy of pain were elucidated recently[51-53]. However, the central mechanism underpinning odor-induced analgesia remains largely unexplored. Here, we report that the odorant molecule 2MT produces robust analgesic effects, leading us to identify a specific olfactory-driven corticothalamic circuit that underlies this phenomenon.

The PC, as the largest cortical region receiving direct olfactory bulb projections, comprises anatomically and functionally distinct APC and PPC subdivisions. The APC receives denser inputs from the olfactory bulb and associated olfactory regions, and is considered critical for odor identification and discrimination[54-56]. In contrast, the PPC forms stronger connections with higher-order associative areas, serving as a key node in odor-guided spatial memory systems[57]. In our study, the fold change in 2MT-evoked neural activation (relative to water control) was significantly greater in the APC than in the PPC. Furthermore, we found that APC^{GABA} neurons were more strongly recruited by the fear odor compared to a neutral odor, whereas APC^{GLU} neurons responded similarly to both odor types. Together, these results indicate that APC^{GABA} neurons are specifically involved in encoding the aversive valence of 2MT.

To confirm the key role of APC^{GABA} neurons in innate fear-induced analgesia, we demonstrated that their inhibition significantly disrupts fear analgesia. Furthermore, artificial activation of APC^{GABA} neurons simultaneously recaptures fear-like freezing and analgesia. While the freezing behavior may confound the measurement of acute nociceptive responses measured using classical reflex-based assays, our data from the CPP assay which assesses the affective-motivational

ARTICLE IN PRESS

component of pain without relying on motor reflexes provide additional support for the role of APC^{GABA} neurons in analgesia, particularly within the affective dimension of pain. Conversely, inhibiting these neurons induces pain hypersensitivity and affective aversion in naïve mice, indicating that tonic activity of APC^{GABA} neurons gates pain perception. These results reveal a gate-keeper role of APC inhibitory neurons in pain regulation, in addition to their indispensable role in mediating fear-induced analgesia. To dissociate the fear-analgesia function of APC^{GABA} neurons from a general role in pain modulation, we specifically manipulated 2MT-responseive APC^{GABA} neurons using the TRAP approach. Our data reveal that this subpopulation is both necessary and sufficient for mediating fear analgesia without affecting basal pain sensitivity, establishing that 2MT-responsive APC^{GABA} neurons are essential for innate fear-induced analgesia and are functionally segregated from general nociceptive processing.

The mediodorsal thalamus, which integrates inputs from multiple olfactory structures, is widely perceived as an olfactory thalamus[58,59]. The direct glutamatergic pathway from APC to MD has been previously identified[60,61]. In this study, we dissect a direct inhibitory pathway from the APC to the MD through neural tracing and electrophysiological recordings. This observation aligns with the growing recognition of cortical long-range inhibitory circuits, including APC→olfactory bulb[62], auditory cortex→lateral amygdala[63], and medial prefrontal cortex→retrosplenial cortex pathways[64]. While our findings extend this emerging framework to the APC→MD axis, the relatively sparse anatomical representation of these projecting GABAergic neurons suggests that their contribution may be context-dependent, and the broader functional significance of this pathway remains to be further defined.

Based on retrograde labeling and Fos staining data, we observed that MD-projecting GABAergic neurons represent a small proportion of all 2MT-activatied neurons. However, ~78% of this specific subpopulation was activated by 2MT. Methodologically, this low numerical representation may partly reflect inherent constrains of retrograde tracing, as some MD-projecting neurons may have been activated but not labeled. Biologically, the high activation rate within this subpopulation suggests functional specificity rather than weak circuit engagement. These findings

ARTICLE IN PRESS

indicate that, although numerically limited, a distinct subset of MD-projecting APC^{GABA} neurons is preferentially recruited by 2MT and exerts a functional influence on fear-related analgesia. In the somatosensory system, the MD is also involved in pain processing[65-67]. We demonstrated that MD neurons underwent maladaptive hyperexcitability in neuropathic pain condition. More interestingly, neuropathic pain-associated hyperactive MD can be rescued by fear odor exposure. We speculate that the APC-MD circuit is the putative interaction substrate for innate fear and pain. Indeed, this rescue effect was precluded by silencing MD-presynaptic APC^{GABA} neurons. Moreover, the pain suppression by innate fear was abrogated when we silence MD-presynaptic APC^{GABA} neurons. It should be noted that while the retro-Cre approach effectively targets MD-projecting neurons, it cannot exclude the possibility of collateral projections to other brain regions. Importantly, our optogenetic inhibition of APC neural terminals within the MD recapitulated the behavioral phenotypes observed during suppression of MD-presynaptic APC^{GABA} neurons, demonstrating the functional specificity of this pathway. Furthermore, chemogenetic inhibition of the entire APC-MD GABAergic terminals not only abolished the analgesic effect of 2MT but also consistently induced pain hypersensitivity in naïve mice. Thus, this pathway plays a dual role in pain modulation: it mediates fear-induced analgesia and provides a tonic inhibitory tone that continuously gates basal nociceptive transmission, as its inhibition alone was sufficient to induce pain hypersensitivity. It remains to be studied whether the APC-MD pathway engages descending pain facilitation systems to mediate innate fear-induced analgesia[68]. In the present study, although we did not observe direct projections from APC^{GABA} neurons to the amygdala, amygdala-centered pathways may still contribute to innate fear-driven analgesia. For instance, the central extended amygdala – a hub for threat integration and response – sends substantial outputs to key pain-modulatory regions, including the periaqueductal gray (PAG), ventral tegmental area (VTA), dorsal raphe nucleus (DRN), and locus coeruleus (LC))[38,69,70].

Fear and pain represent distinct aversive interceptive experiences that drive adaptive threat-avoidance behaviors[71,72]. Our findings demonstrate that innate fear actively suppresses pain perception, but not vice versa, revealing a unidirectional hierarchical relationship between these

ARTICLE IN PRESS

two competing states. By dissecting the neural substrate for ranking these two states, this study provides mechanistic insight into how the brain makes the most adaptive behavioral choice. More importantly, these findings highlight the APC^{GABA}→MD pathway as a potential therapeutic target for modulating maladaptive pain states.

Limitations of the study

This study has several limitations that should be considered when interpreting the results. First, we utilized a VGAT promoter-based viral system to target GABAergic neurons in the APC. Potential off-target effects cannot be fully excluded. Second, our investigation focused primarily on the role of APC^{GABA} neurons in fear-induced analgesia; the potential contribution of 2MT-responsive APC^{GLU} neurons within this circuit remains to be elucidated. Third, given the known local feedback and feedforward inhibition within the PC[73,74], further work is required to determine whether fear-induced analgesia involves local interactions between excitatory and inhibitory neurons or engages disynaptic pathways via long-range excitatory inputs that recruit MD-projecting APC^{GABA} neurons. Finally, altered motor states like freezing can confound movement-dependent pain assessments. Therefore, integrating movement-independent readouts, such as facial grimace scales, will help to achieve a more comprehensive understanding of pain modulation by the APC→MD circuit.

ARTICLE IN PRESS

ARTICLE IN PRESS

Methods

Animals. Adult (8–10 weeks) *C57BL/6J, FosTRAP2,* and *Rosa26-tdTomato (Ai14)* male mice were used in the experiments. *C57BL/6J* mice were purchased from Beijing Vital River Laboratory Animal Technology. *CaMKII-Cre* STOCK B6.Cg-Tg(Camk2a-cre)T29-1Stl/J (IMSR_JAX:005359), *VGAT-Cre* STOCK B6J.129S6(FVB)Slc32a1tm2(cre)Lowl/MwarJ (IMSR_JAX:028862), and *Ai14* STOCK B6;129S6-Gt(ROSA)26Sortm14(CAGtdTomato)Hze/J (IMSR_JAX:007914) mice were initially purchased from Jackson Laboratories. *FosTRAP2* STOCK Fostm2.1(icre/ERT2)Luo/J (Trap2) (IMSR_JAX:030323) mice were gifted by Dr. Shenbin Liu (Fudan University, China). To generate *TRAP2::Ai14* mice for activity-dependent labeling experiments, *FosTRAP2* mice were crossed with *Ai14* mice. All mice were housed in groups of three to five mice per cage with free access to water and food in a biorhythm of 12 h light/12 h dark. The room temperature was kept at 23±1 °C and a consistent humidity of 50 ± 5%. All animal procedures and protocols were approved by the Animal Care and Use Committee of the University of Science and Technology of China.

Stereotaxic injection. The mice were administered intraperitoneal (i.p.) injections of pentobarbital sodium at a dosage of 20 mg/kg, and were then carefully positioned and adjusted on a stereotactic device (RWD Life Technologies Co., Ltd., China). To maintain the body temperature of the mice, a heating pad was utilized. Additionally, eye ointment was applied to protect the mice's eyes from any potential light irritation. A glass micropropipette was utilized for injecting the viruses which are packaged and obtained by BrainVTA (Wuhan, China) in a volume of (300-320 nl for APC and 200-220 nl for MD) at a speed of 50 nl/min. After the injection, the micropipette was left in place for 10 minutes, allowing the virus to spread. Once the mice had recovered from the anesthesia, they were returned to home cages. Behavioral tests were performed 2-3 weeks later. The coordinates were defined as anterior-posterior (AP) from bregma, mediolateral (ML) from the midline, and dorsoventral (DV) from the brain surface (in mm).

Virus injection and optical fiber implantation. To manipulate APC^{GABA} neurons, an adeno-

ARTICLE IN PRESS

associated virus (AAV) carrying the inhibitory hM4Di receptor under the control of the GABAergic neuron promoter (rAAV2/9-VGAT1-hM4D(Gi)-mCherry-WPRE-pA, 5.07E+12 vg/ml, Cat. No. PT-0488) or the excitatory hM3Dq receptor (rAAV2/9-VGAT1-hM3D(Gq)-mCherry-WPRE-pA, 5.44E+12 vg/ml, Cat. No. PT-0489) or rAAV2/9-VGAT1-mCherry-WPRE-pA (5.36E+12 vg/ml, Cat. No. PT-0325) as control were injected into the APC (AP, +0.75 mm; ML, ± 3.25 mm; DV, -5.2 mm) bilaterally.

To inhibit MD-projecting APC^{GABA} neurons, rAAV2/Retro-hSyn-CRE-WPRE-hGH-pA (5.22E+12 vg/ml, Cat. No. PT-2334) was injected into the MD (AP, -1 mm; ML, ±0.5 mm; DV, -3.3 mm) of *C57* mice bilaterally, and rAAV2/9-VGAT1-DIO-hM4D(Gi)-mCherry-WPRE-hGH-pA (5.02E+12 vg/ml, Cat. No. PT-0618) or rAAV2/9-VGAT1-DIO-mCherry-WPRE-hGH-pA (5.79E+12 vg/ml, Cat. No. PT-3225) was injected into the APC bilaterally.

To optogenetically manipulate APC^{GABA} terminals within the MD, rAAV2/9-VGAT1-eNpHR3.0-EYFP-WPRE-hGH-pA (5.00E+12 vg/ml, Cat. No. PT-0182) or rAAV2/9-VGAT1-hChR2(H134R)-mCherry-WPRE-hGH-pA (5.66E+12 vg/ml, Cat. No. PT-0643) were injected into the APC bilaterally. rAAV2/9-VGAT1-EYFP-WPRE-hGH-pA (5.33E+12 vg/ml, Cat. No. PT-0190) or rAAV2/9-VGAT1-mCherry-WPRE-pA (5.44E+12 vg/ml) was used as controls.

To verify the specificity of the VGAT-promoter driven viruses, we injected a mixture of rAAV2/9-DIO-EYFP (5.14E+12 vg/ml, Cat. No. PT-0012) and rAAV2/9-VGAT1-mCherry-WPRE-pA viruses (1:1) into the bilateral APC of *VGAT-Cre* mice.

Fiber photometry. To assess calcium changes, rAAV2/9-hSyn-GCaMp6m-WPRE-hGH-pA (300 nl, 5.14E+12 vg/ml, Cat. No. PT-0148), rAAV2/9-VGAT1-GCaMp6m-WPRE-hGH-pA (300 nl, 5.79E+12 vg/ml, Cat. No. PT-3317), or rAAV2/9-CaMKⅡa-GCaMp6m-WPRE-hGH-pA (300 nl, 5.04E+12 vg/ml, Cat. No. PT-0111) was injected into the APC (AP, +0.75 mm; ML, -3.25 mm; DV, -5.2 mm) unilaterally in *C57* mice. Additionally, rAAV2/9-DIO-GCaMP6m-WPRE-pA (300 nl, 6.21E+12 vg/ml, Cat. No. PT-0283) was injected into the APC of *VGAT-Cre* or *CaMKII-Cre* mice. Two weeks later, the optical fiber (diameter: 200 μm; N.A.: 0.37; length: 5.5 mm; Inper, China) was embedded at the APC by attaching dental cement to the skull. After a one-week

ARTICLE IN PRESS

recovery, Ca^{2+} signals of APC were recorded by the three-color single-channel fiber photometry system (ThinkerTech, China).

Mice were initially placed in a square box and allowed habituation for 30 minutes. During the fiber photometry experiments, odor stimuli—including water, anisole (Sigma, Cat. No. 296295), and 2MT (Tokyo Chemical Industry, Cat. No. M0285) were presented via air puff or cotton swab. Each odor was tested across six repeated trials with 1-minute inter-trial intervals. In each trial, mice were exposed to the odor for 1 second. For air-puff or cotton swab delivery, a Pasteur pipette or a cotton swab containing 50 μl of the odor solution was manually introduced into the chamber for 1 second. By clicking the Mark button on the software (ThinkerTech, China) at the moment when the odorant stimuli were delivered, the behavioral and fluorescent events could be time-locked. The fluorescence signal of each mouse was analyzed six times.

Neurons and terminals expressing GCaMP6m were stimulated by laser intensity at 470 nm wavelength (40 μW) to obtain calcium-dependent fluorescence signals, while motion artifacts were corrected by laser signal at 410 nm (20 μW). The obtained calcium signal was analyzed by MATLAB software and calculated (F−F0)/ F0 (average baseline fluorescence signal) to calculate the changed value of the Ca2+ signal (ΔF/F). The 5-second window around the event was analyzed, using a 2-second window before the stimulus as the baseline. The result was the averaged data from the first six Ca2+ responses (six trials) of each mouse.

Optogenetic manipulation. To optogenetically manipulate APC^{GABA} terminals within the MD, two weeks after the bilateral virus injection into the APC, the optical fibers (diameter: 200 μm; N.A.: 0.37; length: 4.0 mm; Inper, China) were embedded at the MD by attaching dental cement to the skull bilaterally. One week later, behavioral tests were performed. In experiments, the optical fiber in the mice's heads was connected to the laser source through a sleeve line.

For optogenetic manipulation, the intensity of the blue light (473 nm, 2.5 mW, 10 ms, 20 Hz) or the yellow light (594 nm, 5 mW, 10 ms, 20 Hz) was measured and determined by the photometer and then controlled by the device (QAXK-LASER, ThinkerTech, China). On the first day, mice had their heads interfaced with the laser system but were not exposed to any light stimuli. The

ARTICLE IN PRESS

following day, they underwent distinct exposures to either blue or yellow light stimuli to observe differences in behavioral phenotypes. Mice in the control virus groups had the same stimulation regimen.

In detail, during the entire pain experiment, we initially exposed the neurons or circuits to light for 1 minute to enable control. Following this, we employed a stimulation regimen of 1 minute ON and 5 minutes OFF to assess mechanical and thermal sensitivity. During the ON phase, we conducted the necessary measurements. Afterward, the mice were given a 5-minute rest before we repeated the aforementioned steps. For the hot plate test, we used the 3 minutes ON and 5 minutes OFF stimulation regimen.

Chemogenetic manipulation. To manipulate the activity of specific neurons, mice expressing chemogenetic viruses were intraperitoneally injected with CNO (2 mg/kg, APExBIO Technology LLC, Cat. No. A3317) prior to the experiment. After a period of 30 minutes, during which the drug became effective, behavioral experiments were conducted. In the actual experimental procedure, mice are initially administered saline intraperitoneally on the first day to assess their behavioral phenotypes. On the following day, CNO is injected intraperitoneally into the mice to evaluate any differential behavioral phenotypes.

Innate fear detection. In experiments to test the fear, the proportion of the freezing time, the movement distance, and the behavior adjacent to the odor were chosen as indicators to detect fear. To conduct these experiments, the mice were placed in a square glass box lined with clean filter paper. The mice were allowed to acclimate to the apparatus for 30 minutes the day before the innate fear-associated experiments. On the day of the experiment, the mice were initially placed in the box to explore freely for 10 minutes. Then, either water (20 μl), anisole (20 μl), or 2MT (20 μl) was dropped onto the upper left corner of the filter paper using a pipette.The mice were then exposed to the specific odor for 20 minutes. Finally, the proportion of the freezing time and the movement distance, including the trajectory of the mice within the 20-minute period, were analyzed using software (SuperFcs system, XinRuan, Shanghai, China). For data analysis, we

ARTICLE IN PRESS

utilized the built-in SuperMaze animal behavior video analysis software, Version 2.0. This software allowed us to adjust the Mobility/Immobility threshold to accurately differentiate between the mobility and immobility states of the mice, as well as modify the Immobility/Freezing threshold to effectively distinguish between immobility and freezing states induced by fear.

After conducting multiple tests, we determined the optimal initial values displayed on the software to be a Mobility/Immobility threshold of 16 and an Immobility/Freezing threshold of 19. Subsequently, we proceeded with the formal experiment. In all freezing-related experiments mentioned in this article, these preset threshold values were consistently used for analysis."

Certain experiments include the quantification of metrics, including the duration of residence in the odor zone and the number of entries into that zone, all of which are processed using SMART V3.0 software.

Timeline for odor delivery. For pain testing experiments, mice were first acclimatized to the behavioral chamber. Following an acclimatization period, a continuous 2MT (or control solvent) odor was initiated by placing a filter paper saturated with the stimulus at the top of the chamber. Pain assays (von Frey, Hargreaves, etc.) began 2 minutes after the onset of odor exposure, and the odor was maintained throughout the entire testing session to ensure animals remained in a sustained state of innate fear during nociceptive measurements.

Complete Freund's adjuvant (CFA) model. To induce chronic inflammation, CFA (10 μl, Sigma, Cat. No. 8. 18752) was injected into the hind paws of the mice. After a period of seven days following the injection, the withdrawal threshold was measured using the von Frey test, while the withdrawal latency was measured using Hargreaves' test. In order to establish a baseline for comparison, mice that received an injection of saline (0.9% NaCl) were used as control subjects.

Spared nerve injury (SNI) model. Mice were anesthetized under the intraperitoneal injection of pentobarbital sodium (20 mg/kg) and then subjected to nerve injury or sham surgery. The skin on the lateral surface of the thigh was cut, and the sciatic nerve was exposed by separating the muscle with a glass minute needle. The common peroneal nerve and tibial nerve were separated from the

ARTICLE IN PRESS

sural nerve and ligated with nonabsorbent 4-0 chromic gut sutures (Ethicon), and the nerve 2-4 mm distal to the ligation site was resected. In the sham operation, the sciatic nerve and its three branches were exposed, but the nerve was not ligated. Fourteen days after surgery, the withdrawal threshold and withdrawal latency were measured by the von Frey test and Hargreaves' test, respectively.

Inflammatory pain measurement (Formalin test). Mice were placed in a square glass box and allowed to acclimate for 10 minutes. A solution of formalin (10%, Xinhongfu Biotechnology) was prepared, which was then diluted to a 1% concentration using normal saline. Subsequently, the diluted solution (50 μl) was injected subcutaneously into the hind paw of each mouse The licking behavior of the mice was then videotaped with a camera immediately after injection. The number of licking episodes in one hour was recorded. The experiment was divided into two phases. The first phase, known as the acute phase, is comprised of the initial ten minutes. The second phase, referred to as the inflammatory phase, consisted of the remaining 50 minutes.

Mechanical sensitivity measurement (von Frey test). On the day of the behavioral experiment, the mice were initially acclimated to the plexiglass chambers (6.5 x 6.5 x 6 cm) and placed on a wire mesh for one hour. The Up-Down method was employed for the experiment[75]. Briefly, a series of von Frey filaments (North Coast Medical Inc., USA) were used to stimulate the plantar area of the hind paw for a duration of 3 seconds. The responses of the mice to each monofilament were recorded. Each monofilament was tested five times. There was a minimum interval of 5 minutes between each measurement. The stimulus strength that produced a 50% response rate was determined and taken as the withdrawal threshold.

Thermal sensitivity measurement (Hargreaves' test). On the day of the behavioral experiment, the mice were initially given a one-hour period to acclimate to the plexiglass chambers, which measured 6.5 x 6.5 x 6 cm, on the Hargreaves' Apparatus (IITC Life Science Inc., CA, USA). During the experiment, a radiant heat beam emitted by the machine was focused on the hind paws of the mice. Each mouse was subjected to a total of five exposures to the radiant heat beam, and

ARTICLE IN PRESS

the incubation period of paw withdrawal was carefully recorded. To ensure accurate data, there was a minimum interval of 10 minutes between each experiment. In order to prevent tissue damage and minimize the potential for pain sensitization, the duration of the radiant heat beam exposure was limited to a maximum of 20 seconds.

Acute thermal pain measurement (Hot plate test). The mice were placed on a hot plate (IITC Life Science Inc., CA, USA) at a temperature of 47 °C, and both the latency (time taken to respond) and episodes of nocifensive responses (such as jumping and licking) were carefully recorded. To avoid potential tissue damage, the duration of the 47 °C hot plate test was limited to 3 minutes. The control group was exposed to a temperature of 25 °C.

Acute mechanical pain measurement (Pinprick Test). The hind paw of the mice was gently stimulated ten times with a blunt needle that wouldn't pierce or injure the skin. There was at least a one-minute interval between the each stimulation. The number of paw withdrawal reactions was recorded during these ten experiments, and the percentage of reactions was calculated as: (number of paw lifts)/(total trials [n=10]) × 100%.

Rotarod Test. Mice were tested on an accelerated rotary rod (IITC Life Science Inc., CA, USA). The training phase spanned the first two days, during which the mice were trained to maintain balance. The starting speed at 5 rounds per minute, gradually reaching a maximum speed of 20, and the duration of each training session was 5 minutes. On the third day, the test phase began, with the starting speed set at 5 and the maximum speed set to 40. The experimental duration was 5 minutes, during which the instrument automatically recorded the time it took for the mice to drop. The experiment was repeated twice, and the average value was calculated.

Balance beam. The balance beam test was performed using a 1-meter-long beam with a 12 mm wide flat surface, positioned 50 cm above the bench and supported by two rods. A black box containing nesting material from the home cage was placed at the far end of the beam to serve as an incentive. Mice were acclimatized to the apparatus for at least two days prior to testing. A

ARTICLE IN PRESS

refresher training session was conducted approximately 10 minutes before the formal test. If a mouse stalled, sniffed, or failed to advance, it was gently encouraged from behind using a gloved finger. It is worth noting that overtraining could increase stalling behavior due to overfamiliarity with the task. Conversely, mice that failed to traverse the beam after two training days received additional training. Once a mouse entered the black box, it remained there for approximately 15 seconds before the next trial. On the test day, the time taken to cross the beam (s) was recorded for each animal. The apparatus was cleaned with water and 75% ethanol after each trial to remove urine and feces.

Withdrawal kinetics. Withdrawal kinetics were assessed by applying gentle mechanical stimulation to the mouse hind paw using a blunt needle that did not puncture the skin. The response was recorded with slow-motion video, and the maximum vertical distance (mm) the stimulated paw was lifted from the ground was measured. The time (s) from initial lift-off to the highest point of withdrawal was also recorded. Based on these parameters, the paw withdrawal velocity (mm/s) was calculated. Three trials were conducted per mouse, and the average value was determined.

Grip strength. Grip strength was assessed using a grip strength meter (BIOSEB, EB Instruments). Each mouse was positioned on a metal grid and allowed to stabilize. The tail was then gently and steadily pulled backward along the plane of the grid until all four limbs were completely released. The peak grip force (g) displayed on the device was recorded. Sixteen consecutive trials were performed per animal, and the mean grip strength was calculated based on the last 12 trials (trials 5–16).

Conditional place avoidance and preference (CPA/CPP) test. The experimental setup consisted of two chambers with distinct visual cues: one chamber had black walls with black ground, while the other chamber had white walls with white ground. There was also a neutral middle area between the two chambers. The mice were allowed to move freely between the chambers, and their positions were recorded using an overhead camera. On the first day of the experiment, mice were acclimated to the device for 30 minutes, allowing the mice to familiarize themselves with the

ARTICLE IN PRESS

chambers and the visual cues. On day 2, the mice were given a 10-minute period to freely explore the entire device. During this exploration period, the time spent by each mouse in each chamber was recorded.

On days 3, 4, and 5, the mice underwent training sessions. For the CPA test, mice were placed in the white box with no light or saline injection for a duration of 30 minutes on the morning of the training day. Four hours later, mice were placed in the black box and were exposed to either yellow light stimulation or received an injection of CNO. For the CPP test, mice were kept in the black box with no light or saline injection. Four hours later, mice were placed in the white box and were subjected to blue light stimulation or CNO injection.

On day 6, mice were once again given a 10-minute period to freely explore the entire apparatus, and the time they spent in each chamber was recorded. The changes in position preference of mice before and after training were analyzed.

Activity-dependent Fos induction by innate fear. 4-hydroxytamoxifen (4-OHT, Sigma, Cat. No. H6278) was dissolved in ethanol at a concentration of 20 mg/mL and shaken at 37 °C for 15 minutes, after which the solution was aliquoted and stored at -20 °C. Before use, 4-OHT was re-dissolved in ethanol by shaking at 37 °C for 15 minutes, followed by the addition of corn oil to obtain a final 4-OHT concentration of 10 mg/mL. Finally, the ethanol was removed by vacuum evaporation through centrifugation prior to use.

To label neurons specifically activated by innate fear odor 2MT, mice were housed individually before the odor exposure experiment. On the day of the experiment, 2MT solution (20 μl) was applied to filter papers, with H2O (20 μl) or anisole (20 μl) used for the control group. These filter papers were then placed in the cages for 1.5 hours. Subsequently, the mice received an intraperitoneal injection of 4-OHT at a dosage of 50 mg/kg in a final concentration of 10 mg/ml and were exposed to 2MT for an additional 1.5 hours. One week later, the brains of these mice were harvested for further analysis.

For the 2MT re-exposure experiment, *TRAP2::Ai14* mice were acclimated to the experimental environment for two days prior to the initial exposure. On the day of the first exposure, the mice

ARTICLE IN PRESS

were exposed to 2MT (20 μL) for a duration of 3 hours. At 1.5 hours after the start of this exposure, 4-OHT (50 mg/kg) was administered by intraperitoneal injection. One week later, the re-exposure experiment was conducted, with the mice again being adapted to the environment for two days beforehand. During this re-exposure experiment, one group of mice received 2MT (20 μL) and another group received anisole (20 μL) for a period of 3 hours. Following the completion of the odor exposure, the brains were perfused for c-Fos staining.

Immunofluorescence and imaging. Mice were deeply anesthetized with isoflurane and perfused transcardially with 0.1 M PBS (phosphate-buffered saline) followed by PFA (4% paraformaldehyde). Dissected brain tissues were fixed in 4% PFA for an overnight period and then transferred to the sucrose (30%) at 4 °C. After the brains were dehydrated completely by sinking in sucrose, the brains were frozen in Tissue-Tek O.C.T (From SAKURA) and sectioned coronally (35 μm) with the freezing microtome (Leica CM1950, Leica Biosystems). The obtained sections were washed three times with PBS (at least five minutes each) and then incubated with blocking buffer (10% sheep serum in PBS plus 0.3% Triton X-100 in PBS) for one hour at room temperature. Brain sections were incubated with primary antibodies (Rabbit anti-GABA, 1:500, Sigma, Cat. No. A2052; Rabbit anti-c-Fos, 1:500, Synaptic Systems, Cat. No. 226 003) in the blocking buffer overnight at 4 °C. After washing three times with PBS the next day, brain sections were incubated with secondary antibodies (Goat anti-rabbit Alexa Fluor 488, 1:1000, Jackson, Cat. No. 111-545-003) for two hours in the blocking buffer. In the end, the sections were washed again three times with PBS, and then stained with DAPI, washed, mounted, and sealed after dropping anti-fluorescence quench. Immunostained brain sections were subjected to acquisition imaging using the Olympus FV3000 microscope.

Images obtained by laser confocal microscopy were analyzed using Image J or Adobe Photoshop. To quantify the cell proportion of c-Fos positive neurons or anti-GABA-positive neurons in the PC, three to five randomly selected brain sections were chosen for analysis. Dual-color fluorescence was quantified as above. The final percentage for each result was the average percentage of slices in each mouse.

ARTICLE IN PRESS

Fluorescence in situ hybridization (FISH). On the first day, brain slices are washed in DEPC-PBS for 5 minutes, followed by a 5-minute wash in DEPC-PTW (0.1% Tween-20 in PBS), and then incubated in 2x SSC + 0.5% Triton X-100 for 30 minutes. This is followed by two 5-minute washes in DEPC-PTW, after which the slices are incubated in 3% hydrogen peroxide-methanol for 10 minutes to block endogenous peroxidase activity, and then washed twice for 5 minutes in DEPC-PBS. The tissues are then incubated for 10 minutes in triethanolamine-HCl buffer (pH 8.0) containing 0.25% acetic anhydride without ribonuclease to acetylate free amines, followed by three 5-minute washes in DEPC-PBS. The tissue is prehybridized in prehybridization buffer (50% formamide, 25% 2x SSC, 0.3 mg/ml yeast RNA, 0.1 mg/ml heparin, 1x Denhardt's solution, 0.1% Tween-20, 5 mM EDTA) for 2 hours at room temperature, before hybridizing with digoxigenin-labeled antisense cRNA probes for CAMKII (873 bp amplified by primers AGTCTCCAAGCCAACCCC and ATAGAGCGCACACCAGGC from NM_009792.1) and GAD2 (869 bp amplified by primers TCTTTTCTCCTGGTGGCG and AAATCTTGTCCGAGGCGTTCG from NM_008078.1) for 20 hours at 65 °C in the same buffer.

On the second day, the brain slices undergo a 30-minute wash in preheated (65 °C) prehybridization buffer, followed by a 30-minute wash in a 1:1 mixture of preheated (65 °C) prehybridization buffer and TBST. Next, there are two 5-minute washes in TBST, a brief wash in a 1:1 mixture of TBST and TAE, and three 5-minute washes in TAE. Unbound probes are removed by electrophoresis at 60V for 2 hours in a 2% agarose gel, after which the tissue is incubated overnight at 4 °C for 36 hours in Anti-Digoxigenin-POD antibody (Roche, Cat. No. 11207733910), diluted 1:1000 in PBT supplemented with 10% sheep serum.

On the third day, the brain slices are washed three times in TNT buffer, each for 10 minutes, and incubated with anti-IF 488 antibody (Servicebio, Cat. No. G1231), diluted 1:1000 in TBST containing 3% H2O2, for 20 minutes at room temperature, followed by immunofluorescence staining using antibodies against Chk pAb to mCherry (1:1000, abcam, Cat. No. ab205402) and Goat pAb to Chk IgY labeled with Alexa Fluor 594 (1:500, abcam, Cat. No. ab150172).

Brain slice electrophysiology. Mice were anaesthetized with isoflurane and then perfused with

ARTICLE IN PRESS

ice-cold oxygenated N-Methyl-D-glucamine (NMDG) artificial cerebrospinal fluid (ACSF) (20 mL) that contained (in mM): KCl (2.5), NMDG (93), $NaHCO_3$ (30), NaH_2PO_4 (1.2), glucose (25), HEPES (20), thiourea (2), Na-pyruvate (3), $CaCl_2$ (0.5), Na-ascorbate (5), $MgSO_4$ (10), and glutathione (3) (pH 7.3-7.4, 300-305 mOsm). Coronal slices (300 μm thickness) were then removed to ice-cold oxygenated NMDG-ACSF and sectioned on a vibrating microtome (VT1200s, Leica). The brain slices were transferred to oxygenated NMDG-ACSF at 32 °C for incubation and recovery, followed by oxygenated N-2-hydroxyethylpiperazine-N-2-ethanesulfonic acid (HEPES) ACSF that contained (in mM) 92 NaCl, 2.5 KCl, 1.2 NaH2PO4, 30 NaHCO3, 20 HEPES, 25 glucose, 3 Na-pyruvate, 5 Na-ascorbate, 2 thiourea, 2 CaCl2, 2 MgSO4 and 3 GSH (PH 7.3-7.4, 300-305 mOsm) for more than 1 h at 25 °C. Whole-cell patch-clamp recordings were performed in oxygenated standard ACSF that contained (in mM) 129 NaCl, 1.2 KH2PO4, 3 KCl, 2.4 CaCl2, 3 HEPES, 1.3 MgSO4, 10 glucose, and 20 NaHCO3 (PH 7.3-7.4, 300-310 mOsm, oxygenated with 95% O2 and 5% CO2) at 25 °C.

Patch-clamp electrophysiology data were acquired with a MultiClamp 700B amplifier (Molecular Devices) and Clampfit pClamp 10.0 software. Signals were low-pass filtered at 2 kHz and digitized at 5 kHz using Digidata 1550B (Molecular Devices). The pipette (6-8 MΩ) was pulled by a micropipette puller (P-1000, Sutter instrument) and filled with the internal solution that contained (in mM): 130 K-gluconate, 5 KCl, 4 Na2ATP, 0.5 NaGTP, 20 HEPES, 0.5 EGTA (PH 7.28, 290-300 mOsm). To record an input-output curve of neuronal excitability, 10 pA command current steps with 500 ms pulses were injected from 0 to +150 pA, and the number of action potentials (APs) was quantified for each step. To confirm the efficacy of hM4Di-mediated inhibition and hM3Dq-mediated excitation, CNO (10 μM) was bath-applied. Optical stimulation was delivered using a laser through an optical fiber 200 μm in diameter positioned 0.2 mm from the surface of the brain slice. To confirm the efficacy of ChR2-mediated activation, fluorescently labeled neurons were stimulated with a 473 nm laser using 20 Hz stimulation protocols with a pulse width of 10 ms. In similar, the functional expression of eNpHR3.0 was assessed by applying yellow (594 nm) laser light stimulation.

ARTICLE IN PRESS

To examine functional inhibitory projections from the APC to the downstream regions and sIPSCs of MD neurons, recordings were conducted in the presence of CNQX (10 μM, Sigma) and patch pipettes were filled with the chloride-based internal solution that contained (in mM): 145 CsCl, 10 EGTA, 10 HEPES, 2 MgCl2, 2 CaCl2, 2 Mg-ATP and 5 QX-314. Neurons were held at −70 mV using the voltage clamp for recording inward Cs^+-IPSCs. For evaluating synaptic identities, GABA-mediated IPSCs were blocked by the bath application of bicuculline (10 μM, Sigma, Cat. No. 14343). To test direct synaptic connections, both TTX (1 μM, Sigma, Cat. No. A0224) and 4-AP (500 μM, Sigma, Cat. No. 275875) were used to restore monosynaptic current.

To investigate the effect of 2MT exposure on neuronal excitability, mice were placed in a cage containing 2MT for 1 hour prior to the experiment. Subsequently, they were sacrificed for brain slicing to ensure the sustained effect of the 2MT odor.

To investigate the effect of odor exposure on neuronal excitability, mice were continuously exposed to 2MT or water for 60 minutes by applying 20 μl odorant solutions to filter paper positioned at the testing arena. Acute brain slices containing the MD thalamus were then prepared for electrophysiological recordings.

To investigate the effect of chemogenetic inhibition on neuronal excitability, mice received intraperitoneal CNO injections (30 minutes prior) to either 1-hour 2MT or water exposure, after which acute brain slices containing the MD thalamus were prepared for electrophysiological recordings.

Quantification and statistical analysis. All experiments and data analyses were performed in a double-blind manner. GraphPad Prism v.8.0.1, Olympus FV10-ASW 4.0a Viewer, ImageJ, Clampfit software v.10.0, SuperFcs system, SMART V3.0 software, and MATLAB R2017b software were used to analyze the data. Unpaired Student's t-test (or Mann-Whitney U test), paired Student's t-test (or Wilcoxon signed-rank test), and one-way ANOVA or two-way ANOVA test followed by Bonferroni's test for multiple comparisons were used to determine statistical differences. Shapiro-Wilk test was used to test whether the data followed a normal distribution. When data were normally distributed, paired and unpaired t-tests were implemented. When data

ARTICLE IN PRESS

did not conform to a normal distribution, the Wilcoxon signed-rank test was used for paired comparisons, while the Mann-Whitney U test was used for unpaired comparisons. Results with *P < 0.05, **P < 0.01, ***P < 0.001, ****P < 0.0001 were statistically significant. All data were presented as the mean ± s.e.m except for Supplementary Fig. 6 and 12 shown as box and whisker plots (medians, quartiles (boxes), and ranges from minimum to maximum (whiskers)). Detailed analysis results are shown in Supplementary Data 1.

Data Availability

Source data are provided with this paper. There are no restrictions on data availability in the manuscript.

ARTICLE IN PRESS

ARTICLE IN PRESS

REFERENCES

1 Anderson, D. J. Circuit modules linking internal states and social behaviour in flies and mice. Nature reviews. Neuroscience **17**, 692-704, doi:10.1038/nrn.2016.125 (2016).

2 Flavell, S. W., Gogolla, N., Lovett-Barron, M. & Zelikowsky, M. The emergence and influence of internal states. Neuron **110**, 2545-2570, doi:10.1016/j.neuron.2022.04.030 (2022).

3 Tinbergen, N. The study of instinct. Clarendon Press (1951).

4 Fanselow, M. S. Conditioned fear-induced opiate analgesia: a competing motivational state theory of stress analgesia. Annals of the New York Academy of Sciences **467**, 40-54, doi:10.1111/j.1749-6632.1986.tb14617.x (1986).

5 Alhadeff, A. L. et al. A Neural Circuit for the Suppression of Pain by a Competing Need State. Cell **173**, 140-152 e115, doi:10.1016/j.cell.2018.02.057 (2018).

6 Farrell, M. J. et al. Unique, common, and interacting cortical correlates of thirst and pain. Proceedings of the National Academy of Sciences of the United States of America **103**, 2416-2421, doi:10.1073/pnas.0511019103 (2006).

7 Hamm, R. J. & Lyeth, B. G. Nociceptive thresholds following food restriction and return to free-feeding. Physiology & behavior **33**, 499-501, doi:10.1016/0031-9384(84)90176-8 (1984).

8 Hargraves, W. A. & Hentall, I. D. Analgesic effects of dietary caloric restriction in adult mice. Pain **114**, 455-461, doi:10.1016/j.pain.2005.01.010 (2005).

9 Goldstein, N. et al. A parabrachial hub for need-state control of enduring pain. Nature **647**, 689-697, doi:10.1038/s41586-025-09602-x (2025).

10 LaGraize, S. C., Borzan, J., Rinker, M. M., Kopp, J. L. & Fuchs, P. N. Behavioral evidence for competing motivational drives of nociception and hunger. Neuroscience letters **372**, 30-34, doi:10.1016/j.neulet.2004.09.008 (2004).

11 Olango, W. M., Roche, M., Ford, G. K., Harhen, B. & Finn, D. P. The endocannabinoid system in the rat dorsolateral periaqueductal grey mediates fear-conditioned analgesia and controls fear expression in the presence of nociceptive tone. British journal of pharmacology **165**, 2549-2560, doi:10.1111/j.1476-5381.2011.01478.x (2012).

12 Helmstetter, F. J. & Fanselow, M. S. Effects of naltrexone on learning and performance of conditional fear-induced freezing and opioid analgesia. Physiology & behavior **39**, 501-505, doi:10.1016/0031-9384(87)90380-5 (1987).

13 Ford, G. K., Kieran, S., Dolan, K., Harhen, B. & Finn, D. P. A role for the ventral hippocampal endocannabinoid system in fear-conditioned analgesia and fear responding in the presence of nociceptive tone in rats. Pain **152**, 2495-2504, doi:10.1016/j.pain.2011.07.014 (2011).

14 Stegemann, A. et al. Prefrontal engrams of long-term fear memory perpetuate pain perception. Nature neuroscience **26**, 820-829, doi:10.1038/s41593-023-01291-x (2023).

15 Bolles, R. C. & Fanselow, M. S. A perceptual-defensive-recuperative model of fear and pain. Behavioral and Brain Sciences **3**, 291-301, doi:10.1017/S0140525X0000491X (1980).

16 Isosaka, T. et al. Htr2a-Expressing Cells in the Central Amygdala Control the Hierarchy between Innate and Learned Fear. Cell **163**, 1153-1164, doi:10.1016/j.cell.2015.10.047 (2015).

17 Sosulski, D. L., Bloom, M. L., Cutforth, T., Axel, R. & Datta, S. R. Distinct representations of olfactory information in different cortical centres. Nature **472**, 213-216, doi:10.1038/nature09868 (2011).

ARTICLE IN PRESS

ARTICLE IN PRESS

18 Wilson, D. A. & Sullivan, R. M. Cortical processing of odor objects. Neuron **72**, 506-519, doi:10.1016/j.neuron.2011.10.027 (2011).

19 Bekkers, J. M. & Suzuki, N. Neurons and circuits for odor processing in the piriform cortex. Trends in neurosciences **36**, 429-438, doi:10.1016/j.tins.2013.04.005 (2013).

20 Choi, G. B. et al. Driving opposing behaviors with ensembles of piriform neurons. Cell **146**, 1004-1015, doi:10.1016/j.cell.2011.07.041 (2011).

21 Terral, G. et al. CB1 Receptors in the Anterior Piriform Cortex Control Odor Preference Memory. Current biology : CB **29**, 2455-2464 e2455, doi:10.1016/j.cub.2019.06.041 (2019).

22 Meissner-Bernard, C., Dembitskaya, Y., Venance, L. & Fleischmann, A. Encoding of Odor Fear Memories in the Mouse Olfactory Cortex. Current biology : CB **29**, 367-380 e364, doi:10.1016/j.cub.2018.12.003 (2019).

23 Kondoh, K. et al. A specific area of olfactory cortex involved in stress hormone responses to predator odours. Nature **532**, 103-106, doi:10.1038/nature17156 (2016).

24 Matsukawa, M., Yoshikawa, M., Katsuyama, N., Aizawa, S. & Sato, T. The Anterior Piriform Cortex and Predator Odor Responses: Modulation by Inhibitory Circuits. Frontiers in behavioral neuroscience **16**, 896525, doi:10.3389/fnbeh.2022.896525 (2022).

25 Wang, L. et al. Cell-Type-Specific Whole-Brain Direct Inputs to the Anterior and Posterior Piriform Cortex. Frontiers in neural circuits **14**, 4, doi:10.3389/fncir.2020.00004 (2020).

26 Blanchard, R. J. & Blanchard, D. C. Passive and active reactions to fear-eliciting stimuli. Journal of comparative and physiological psychology **68**, 129-135, doi:10.1037/h0027676 (1969).

27 Takahashi, L. K., Nakashima, B. R., Hong, H. & Watanabe, K. The smell of danger: a behavioral and neural analysis of predator odor-induced fear. Neuroscience and biobehavioral reviews **29**, 1157-1167, doi:10.1016/j.neubiorev.2005.04.008 (2005).

28 Guenthner, C. J., Miyamichi, K., Yang, H. H., Heller, H. C. & Luo, L. Permanent genetic access to transiently active neurons via TRAP: targeted recombination in active populations. Neuron **78**, 773-784, doi:10.1016/j.neuron.2013.03.025 (2013).

29 Kurahashi, T. & Menini, A. Mechanism of odorant adaptation in the olfactory receptor cell. Nature **385**, 725-729, doi:10.1038/385725a0 (1997).

30 Johansen, J. P. & Fields, H. L. Glutamatergic activation of anterior cingulate cortex produces an aversive teaching signal. Nature neuroscience **7**, 398-403, doi:10.1038/nn1207 (2004).

31 Benarroch, E. E. Involvement of the nucleus accumbens and dopamine system in chronic pain. Neurology **87**, 1720-1726, doi:10.1212/WNL.0000000000003243 (2016).

32 Massaly, N. et al. Pain-Induced Negative Affect Is Mediated via Recruitment of The Nucleus Accumbens Kappa Opioid System. Neuron **102**, 564-573 e566, doi:10.1016/j.neuron.2019.02.029 (2019).

33 Ji, Y. W. et al. Plasticity in ventral pallidal cholinergic neuron-derived circuits contributes to comorbid chronic pain-like and depression-like behaviour in male mice. Nature communications **14**, 2182, doi:10.1038/s41467-023-37968-x (2023).

34 Labrakakis, C. The Role of the Insular Cortex in Pain. International journal of molecular sciences **24**, doi:10.3390/ijms24065736 (2023).

35 Wang, X. Y. et al. The thalamic reticular nucleus-lateral habenula circuit regulates depressive-like behaviors in chronic stress and chronic pain. Cell reports **42**, 113170, doi:10.1016/j.celrep.2023.113170 (2023).

36 Gehrlach, D. A. et al. A whole-brain connectivity map of mouse insular cortex. eLife **9**,

ARTICLE IN PRESS

ARTICLE IN PRESS

doi:10.7554/eLife.55585 (2020).

37 Kozlowska, K., Walker, P., McLean, L. & Carrive, P. Fear and the Defense Cascade: Clinical Implications and Management. Harvard review of psychiatry **23**, 263-287, doi:10.1097/HRP.0000000000000065 (2015).

38 Fox, A. S., Oler, J. A., Tromp do, P. M., Fudge, J. L. & Kalin, N. H. Extending the amygdala in theories of threat processing. Trends in neurosciences **38**, 319-329, doi:10.1016/j.tins.2015.03.002 (2015).

39 Helmstetter, F. J. The amygdala is essential for the expression of conditional hypoalgesia. Behavioral neuroscience **106**, 518-528, doi:10.1037//0735-7044.106.3.518 (1992).

40 Corcoran, L., Mattimoe, D., Roche, M. & Finn, D. P. Attenuation of fear-conditioned analgesia in rats by monoacylglycerol lipase inhibition in the anterior cingulate cortex: Potential role for CB(2) receptors. British journal of pharmacology **177**, 2240-2255, doi:10.1111/bph.14976 (2020).

41 Fanselow, M. S. Odors released by stressed rats produce opioid analgesia in unstressed rats. Behavioral neuroscience **99**, 589-592, doi:10.1037//0735-7044.99.3.589 (1985).

42 Dahlhamer, J. et al. Prevalence of Chronic Pain and High-Impact Chronic Pain Among Adults - United States, 2016. MMWR. Morbidity and mortality weekly report **67**, 1001-1006, doi:10.15585/mmwr.mm6736a2 (2018).

43 Chao, C. C. et al. Brain imaging signature of neuropathic pain phenotypes in small-fiber neuropathy: altered thalamic connectome and its associations with skin nerve degeneration. Pain **162**, 1387-1399, doi:10.1097/j.pain.0000000000002155 (2021).

44 Moisset, X. & Bouhassira, D. Brain imaging of neuropathic pain. NeuroImage **37 Suppl 1**, S80-88, doi:10.1016/j.neuroimage.2007.03.054 (2007).

45 Kuner, R. Central mechanisms of pathological pain. Nature medicine **16**, 1258-1266, doi:10.1038/nm.2231 (2010).

46 Wang, X. Y. et al. A glutamatergic DRN-VTA pathway modulates neuropathic pain and comorbid anhedonia-like behavior in mice. Nature communications **14**, 5124, doi:10.1038/s41467-023-40860-3 (2023).

47 Lv, S. S. et al. Corticotropin-releasing hormone neurons control trigeminal neuralgia-induced anxiodepression via a hippocampus-to-prefrontal circuit. Science advances **10**, eadj4196, doi:10.1126/sciadv.adj4196 (2024).

48 Gardner, W. J., Licklider, J. C. & Weisz, A. Z. Suppression of pain by sound. Science **132**, 32-33, doi:10.1126/science.132.3418.32 (1960).

49 Noseda, R. et al. Migraine photophobia originating in cone-driven retinal pathways. Brain : a journal of neurology **139**, 1971-1986, doi:10.1093/brain/aww119 (2016).

50 Peana, A. T. et al. (-)-Linalool produces antinociception in two experimental models of pain. European journal of pharmacology **460**, 37-41, doi:10.1016/s0014-2999(02)02856-x (2003).

51 Tang, Y. L. et al. Green light analgesia in mice is mediated by visual activation of enkephalinergic neurons in the ventrolateral geniculate nucleus. Science translational medicine **14**, eabq6474, doi:10.1126/scitranslmed.abq6474 (2022).

52 Cao, P. et al. Green light induces antinociception via visual-somatosensory circuits. Cell reports **42**, 112290, doi:10.1016/j.celrep.2023.112290 (2023).

53 Zhou, W. et al. Sound induces analgesia through corticothalamic circuits. Science **377**, 198-204, doi:10.1126/science.abn4663 (2022).

54 Miura, K., Mainen, Z. F. & Uchida, N. Odor representations in olfactory cortex: distributed rate coding and

ARTICLE IN PRESS

decorrelated population activity. Neuron **74**, 1087-1098, doi:10.1016/j.neuron.2012.04.021 (2012).

55 Poo, C. & Isaacson, J. S. Odor representations in olfactory cortex: "sparse" coding, global inhibition, and oscillations. Neuron **62**, 850-861, doi:10.1016/j.neuron.2009.05.022 (2009).

56 Iurilli, G. & Datta, S. R. Population Coding in an Innately Relevant Olfactory Area. Neuron **93**, 1180-1197.e1187, doi:10.1016/j.neuron.2017.02.010 (2017).

57 Poo, C., Agarwal, G., Bonacchi, N. & Mainen, Z. F. Spatial maps in piriform cortex during olfactory navigation. Nature **601**, 595-599, doi:10.1038/s41586-021-04242-3 (2022).

58 Courtiol, E. & Wilson, D. A. Thalamic olfaction: characterizing odor processing in the mediodorsal thalamus of the rat. Journal of neurophysiology **111**, 1274-1285, doi:10.1152/jn.00741.2013 (2014).

59 Price, J. L. & Slotnick, B. M. Dual olfactory representation in the rat thalamus: an anatomical and electrophysiological study. The Journal of comparative neurology **215**, 63-77, doi:10.1002/cne.902150106 (1983).

60 Kuroda, M., Lopez-Mascaraque, L. & Price, J. L. Neuronal and synaptic composition of the mediodorsal thalamic nucleus in the rat: a light and electron microscopic Golgi study. The Journal of comparative neurology **326**, 61-81, doi:10.1002/cne.903260106 (1992).

61 Pelzer, P., Horstmann, H. & Kuner, T. Ultrastructural and Functional Properties of a Giant Synapse Driving the Piriform Cortex to Mediodorsal Thalamus Projection. Frontiers in synaptic neuroscience **9**, 3, doi:10.3389/fnsyn.2017.00003 (2017).

62 Mazo, C. et al. Long-range GABAergic projections contribute to cortical feedback control of sensory processing. Nature communications **13**, 6879, doi:10.1038/s41467-022-34513-0 (2022).

63 Bertero, A., Feyen, P. L. C., Zurita, H. & Apicella, A. J. A Non-Canonical Cortico-Amygdala Inhibitory Loop. The Journal of neuroscience : the official journal of the Society for Neuroscience **39**, 8424-8438, doi:10.1523/JNEUROSCI.1515-19.2019 (2019).

64 Dautan, D. et al. Cortico-cortical transfer of socially derived information gates emotion recognition. Nature neuroscience **27**, 1318-1332, doi:10.1038/s41593-024-01647-x (2024).

65 Meda, K. S. et al. Microcircuit Mechanisms through which Mediodorsal Thalamic Input to Anterior Cingulate Cortex Exacerbates Pain-Related Aversion. Neuron **102**, 944-959 e943, doi:10.1016/j.neuron.2019.03.042 (2019).

66 Whitt, J. L., Masri, R., Pulimood, N. S. & Keller, A. Pathological activity in mediodorsal thalamus of rats with spinal cord injury pain. The Journal of neuroscience : the official journal of the Society for Neuroscience **33**, 3915-3926, doi:10.1523/JNEUROSCI.2639-12.2013 (2013).

67 Huang, T. et al. Identifying the pathways required for coping behaviours associated with sustained pain. Nature **565**, 86-90, doi:10.1038/s41586-018-0793-8 (2019).

68 You, H. J., Lei, J. & Pertovaara, A. Thalamus: The 'promoter' of endogenous modulation of pain and potential therapeutic target in pathological pain. Neuroscience and biobehavioral reviews **139**, 104745, doi:10.1016/j.neubiorev.2022.104745 (2022).

69 Lebow, M. A. & Chen, A. Overshadowed by the amygdala: the bed nucleus of the stria terminalis emerges as key to psychiatric disorders. Molecular psychiatry **21**, 450-463, doi:10.1038/mp.2016.1 (2016).

70 Hao, S. et al. The Lateral Hypothalamic and BNST GABAergic Projections to the Anterior Ventrolateral Periaqueductal Gray Regulate Feeding. Cell reports **28**, 616-624 e615, doi:10.1016/j.celrep.2019.06.051 (2019).

ARTICLE IN PRESS

ARTICLE IN PRESS

71 Craig, A. D. Interoception: the sense of the physiological condition of the body. Current opinion in neurobiology **13**, 500-505, doi:10.1016/s0959-4388(03)00090-4 (2003).

72 Adolphs, R. The biology of fear. Current biology : CB **23**, R79-93, doi:10.1016/j.cub.2012.11.055 (2013).

73 Large, A. M., Vogler, N. W., Mielo, S. & Oswald, A. M. Balanced feedforward inhibition and dominant recurrent inhibition in olfactory cortex. Proceedings of the National Academy of Sciences of the United States of America **113**, 2276-2281, doi:10.1073/pnas.1519295113 (2016).

74 Suzuki, N. & Bekkers, J. M. Distinctive classes of GABAergic interneurons provide layer-specific phasic inhibition in the anterior piriform cortex. Cerebral cortex **20**, 2971-2984, doi:10.1093/cercor/bhq046 (2010).

75 Chaplan, S. R., Bach, F. W., Pogrel, J. W., Chung, J. M. & Yaksh, T. L. Quantitative assessment of tactile allodynia in the rat paw. Journal of neuroscience methods **53**, 55-63, doi:10.1016/0165-0270(94)90144-9 (1994).

ARTICLE IN PRESS

ARTICLE IN PRESS

ACKNOWLEDGMENTS: This study was supported by the National Natural Science Foundation of China (grants 32271048, 32571336, 32070999 to Y. Z., grant 82471311 to W. H., and grant 823B2022 to X. Y. W), the Leading Medicine and Advanced Technologies of IHM (grant 2025IHM01100 to Y. Z.) and Anhui Provincial Natural Science Foundation (grant 2008085J16 to Y. Z.).

AUTHOR CONTRIBUTIONS: W. B. J., X. Y. W. and X. X. X. designed the studies and conducted most of experiments and data analysis. L. T., Y. X. L, and X. L. L. were involved in the revision. X. Q. L. managed the mouse colonies used in this study. Y. Z., W. B. J. and X. Y. W. wrote the first draft. W. H. and Y. Z. were involved in the overall design of the project and editing of the final manuscript.

DECLARATION OF INTERESTS

The authors declare no competing interests.

ARTICLE IN PRESS

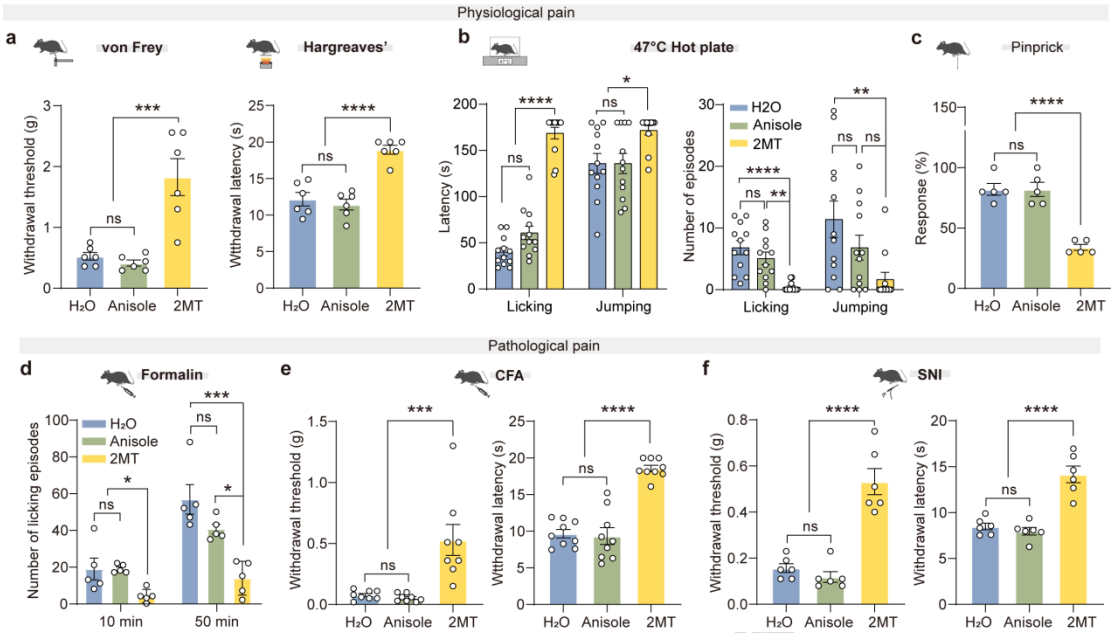

Fig 1. Innate fear odor 2MT induces analgesia.

a, Paw withdrawal threshold in the von Frey test (left) and paw withdrawal latency in the Hargreaves' test (right) of mice exposed to water (H_2O), anisole, or 2MT (n=6 mice/group; von Frey, H_2O vs 2MT, $P = 0.0004$, Anisole vs 2MT, $P = 0.0002$; Hargreaves', $P < 0.0001$). **b**, Latency (left) and number of licking or jumping episodes (right) of mice in the hot plate test (n=12 mice/group; Licking latency, $P < 0.0001$; Jumping latency, H_2O vs 2MT, $P = 0.0279$, Anisole vs 2MT, $P = 0.0275$; Number of licking episodes, H_2O vs 2MT, $P < 0.0001$, Anisole vs 2MT, $P = 0.0021$; Number of Jumping episodes, H_2O vs 2MT, $P = 0.0089$). **c**, The percentage of nocifensive responses to 10 trials of pinprick stimulation (n=5 mice/group, $P < 0.0001$). **d**, Number of paw-licking episodes of mice in the formalin-induced inflammatory model (n=5 mice/group; 10 min, H_2O vs 2MT, $P = 0.0433$, Anisole vs 2MT, $P = 0.0403$; 50 min, H_2O vs 2MT, $P = 0.0004$, Anisole vs 2MT, $P = 0.0135$). **e**, **f**, Paw withdrawal threshold (left) and paw withdrawal latency (right) of mice treated with CFA (**e**, n=9 mice; von Frey, H_2O vs 2MT, $P = 0.0009$, Anisole vs 2MT, $P = 0.0005$; Hargreaves', $P < 0.0001$) or SNI (**f**, n=6 mice, $P < 0.0001$). Significance was assessed by one-way ANOVA with Bonferroni post hoc analysis in (**a-f**). All data are presented as the mean ± s.e.m. $*P < 0.05$, $**P < 0.01$, $***P < 0.001$, $****P < 0.0001$, not significant (ns). Details of the statistical analyses are presented in Supplementary Data 1. Source data are provided as a Source

ARTICLE IN PRESS

Data file.

ARTICLE IN PRESS

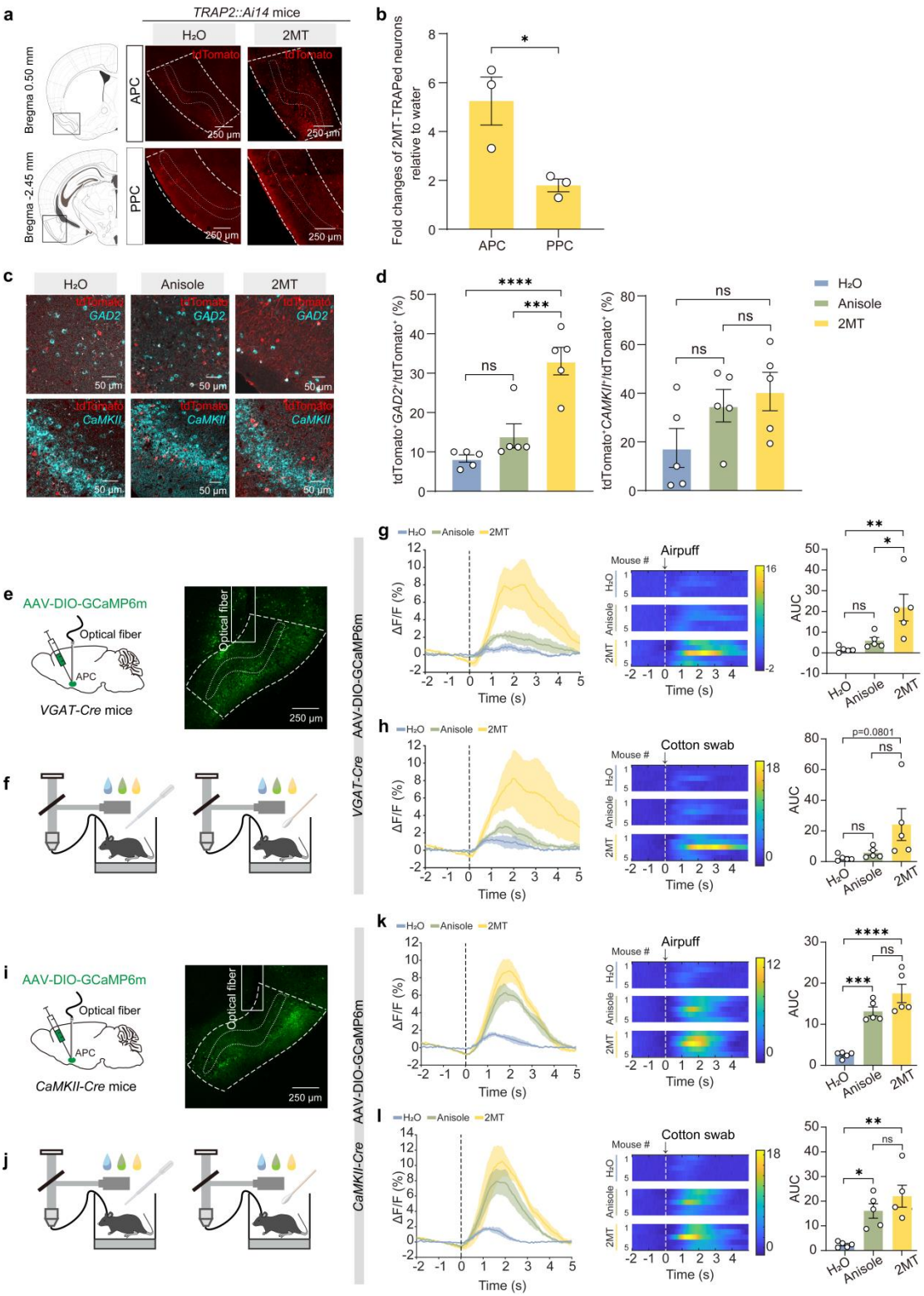

Fig 2. APC^{GABA} neurons respond to innate fear-related olfactory information.

ARTICLE IN PRESS

a, Representative images of tdTomato-positive signals in the APC and PPC of *TRAP2::Ai14* mice exposed to H_2O or 2MT. Scale bar, 250 μm. **b**, Quantification of the fold change in 2MT-induced neural activation relative to the water control (n=21sections from 5 mice/group, $P = 0.0334$). **c**, **d**, Representative images (**c**) and quantification (**d**) showing the percentage of $tdTomato^+$ neurons (red) in the APC which co-localize with fluorescence in situ hybridization (FISH) for inhibitory GABAergic neurons and excitatory glutamatergic neurons (cyan). Scale bar, 50 μm (n=21 sections from 5 mice/group; H_2O vs 2MT, $P < 0.0001$; Anisole vs 2MT, $P = 0.0010$). **e**, **i**, Schematic of the viral injection (left) and optic fiber implantation (right) in *VGAT-Cre* or *CaMKII-Cre* mice. Scale bar, 250 μm. **f**, **j**, Illustration of fiber photometry recording in response to H_2O, anisole, and 2MT delivered via airpuff (left) or cotton swabs (right). **g**, **h**, **k**, **l**, Average responses (left), heatmaps (middle), and AUC during 0–5 s (right) showing Ca^{2+} transients elicited by H_2O, anisole, or 2MT delivered via airpuff (**g**, **k**) or cotton swabs (**h**, **l**) (n=5 mice/group; **g**, H_2O vs 2MT, $P = 0.0075$; Anisole vs 2MT, $P = 0.0303$; **k**, H_2O vs 2MT, $P < 0.0001$; Anisole vs H_2O, $P = 0.0007$; **l**, H_2O vs 2MT, $P = 0.0020$; Anisole vs 2MT, $P = 0.0222$). Significance was assessed by two-tailed unpaired Student's t-test in (**b**), and one-way ANOVA with Bonferroni post hoc analysis in (**d**, **g**, **h**, **k**, **l**). All data are presented as the mean ± s.e.m. $*P < 0.05$, $**P < 0.01$, $***P < 0.001$, $****P < 0.0001$, not significant (ns). Details of the statistical analyses are presented in Supplementary Data 1. Source data are provided as a Source Data file.

ARTICLE IN PRESS

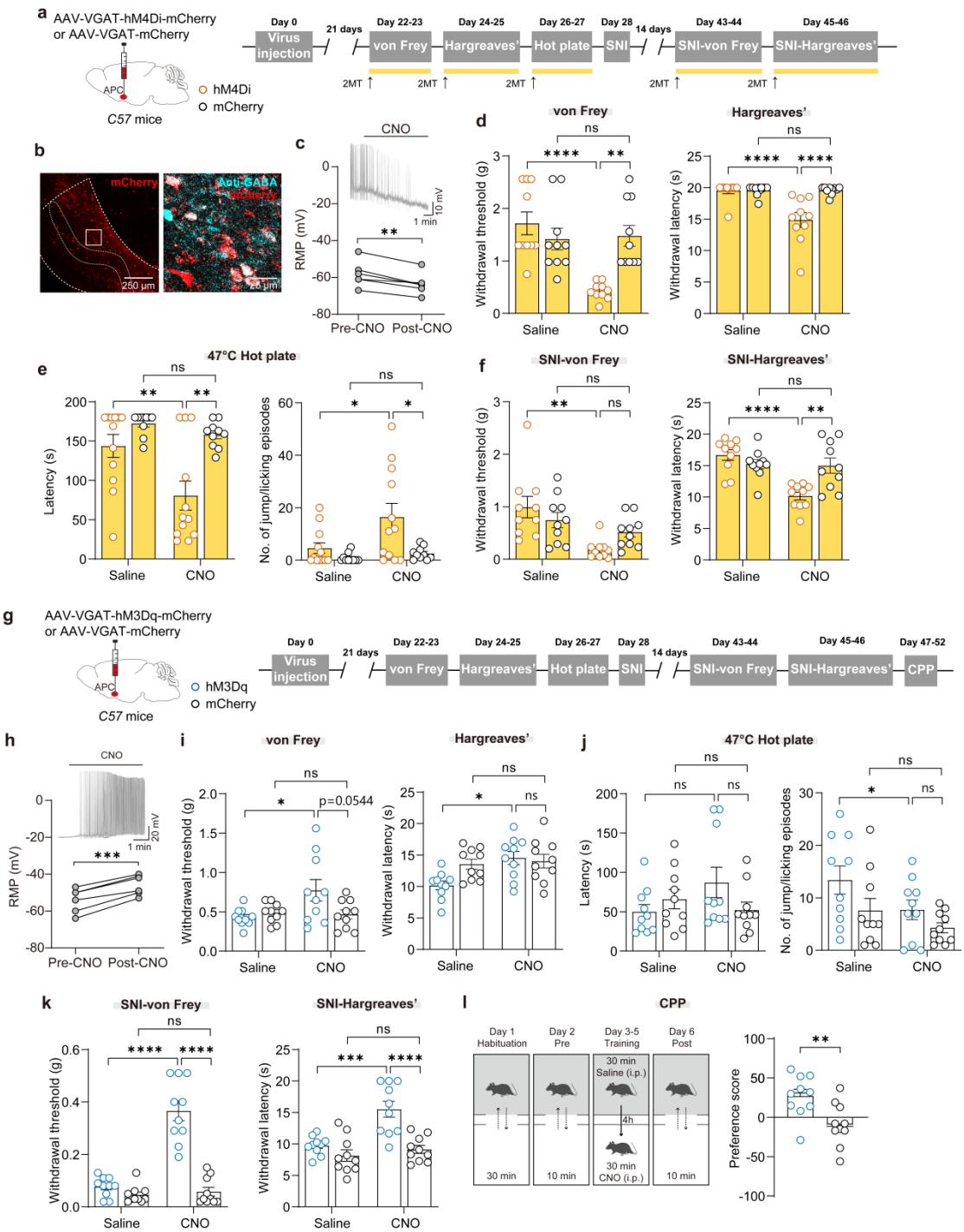

Fig 3.

APC^{GABA} neurons mediate fear-induced analgesia.

a, **g**, Schematic of the viral injection and timeline of the behavioral experiments. **b**, Representative image of mCherry-expressing neurons (red) co-localized with anti-GABA staining (cyan) in the APC (arrow, double-labeled neurons). Scale bars, 250 μm and 25 μm. **c**, Representative trace

ARTICLE IN PRESS

showing hyperpolarization of an hM4Di-expressing neuron after CNO application (top) and quantification of the RMP across multiple animals (bottom) (n=3 mice, $P = 0.0018$). **d-f**, Effects of the chemogenetic inhibition of APC^{GABA} neurons on the basal nociception (**d**: hM4Di, n=10 mice; mCherry, n=10 mice; von Frey, hM4Di&Saline vs hM4Di&CNO, $P < 0.0001$; hM4Di&CNO vs mCherry&CNO, $P = 0.0028$; Hargreaves', $P < 0.0001$), acute thermal pain (**e**: hM4Di, n=12 mice; mCherry, n=10 mice; Latency, hM4Di&Saline vs hM4Di&CNO, $P = 0.0064$; hM4Di&CNO vs mCherry&CNO, $P = 0.0011$; Episodes, hM4Di&Saline vs hM4Di&CNO, $P = 0.0369$; hM4Di&CNO vs mCherry&CNO, $P = 0.0154$) and chronic neuropathic pain (**f**: hM4Di, n=10 mice; mCherry, n=10 mice; von Frey, hM4Di&Saline vs hM4Di&CNO, $P = 0.001$; Hargreaves', hM4Di&Saline vs hM4Di&CNO, $P < 0.0001$; hM4Di&CNO vs mCherry&CNO, $P = 0.0027$) of 2MT-exposed mice. **h**, Representative trace showing depolarization of an hM3Dq-expressing neuron after CNO application (top) and quantification of the RMP across multiple animals (bottom) (n=3 mice, $P = 0.0002$). **i-k**, Effects of the chemogenetic activation of APC^{GABA} neurons on the basal nociception (**i**: hM3Dq, n=10 mice; mCherry, n=10 mice; von Frey, hM3Dq&Saline vs hM3Dq&CNO, $P = 0.0236$; hM3Dq&CNO vs mCherry&CNO, $P = 0.0544$; Hargreaves', $P = 0.0102$), acute thermal pain (**j**: hM3Dq, n=10 mice; mCherry, n=10 mice; Episoldes, $P = 0.0368$) and chronic neuropathic pain (**k**: hM3Dq, n=10 mice; mCherry, n=10 mice; von Frey, $P < 0.0001$; Hargreaves', hM3Dq&Saline vs hM3Dq&CNO, $P = 0.0003$; hM3Dq&CNO vs mCherry&CNO, $P < 0.0001$). **l**, Experimental schematic (left) and quantification (right) of conditioned place preference (CPP) test (n=10 mice/group, $P = 0.0074$). Significance was assessed by two-tailed paired Student's t-test in (**c**, **h**), two-way ANOVA followed by Bonferroni's multiple comparisons test (**d-f**, **i-k**) and two-tailed unpaired Student's t-test in (**l**). All data are presented as the mean ± s.e.m. $*P < 0.05$, $**P < 0.01$, $***P < 0.001$, $****P < 0.0001$, not significant (ns). Details of the statistical analyses are presented in Supplementary Data 1. Source data are provided as a Source Data file.

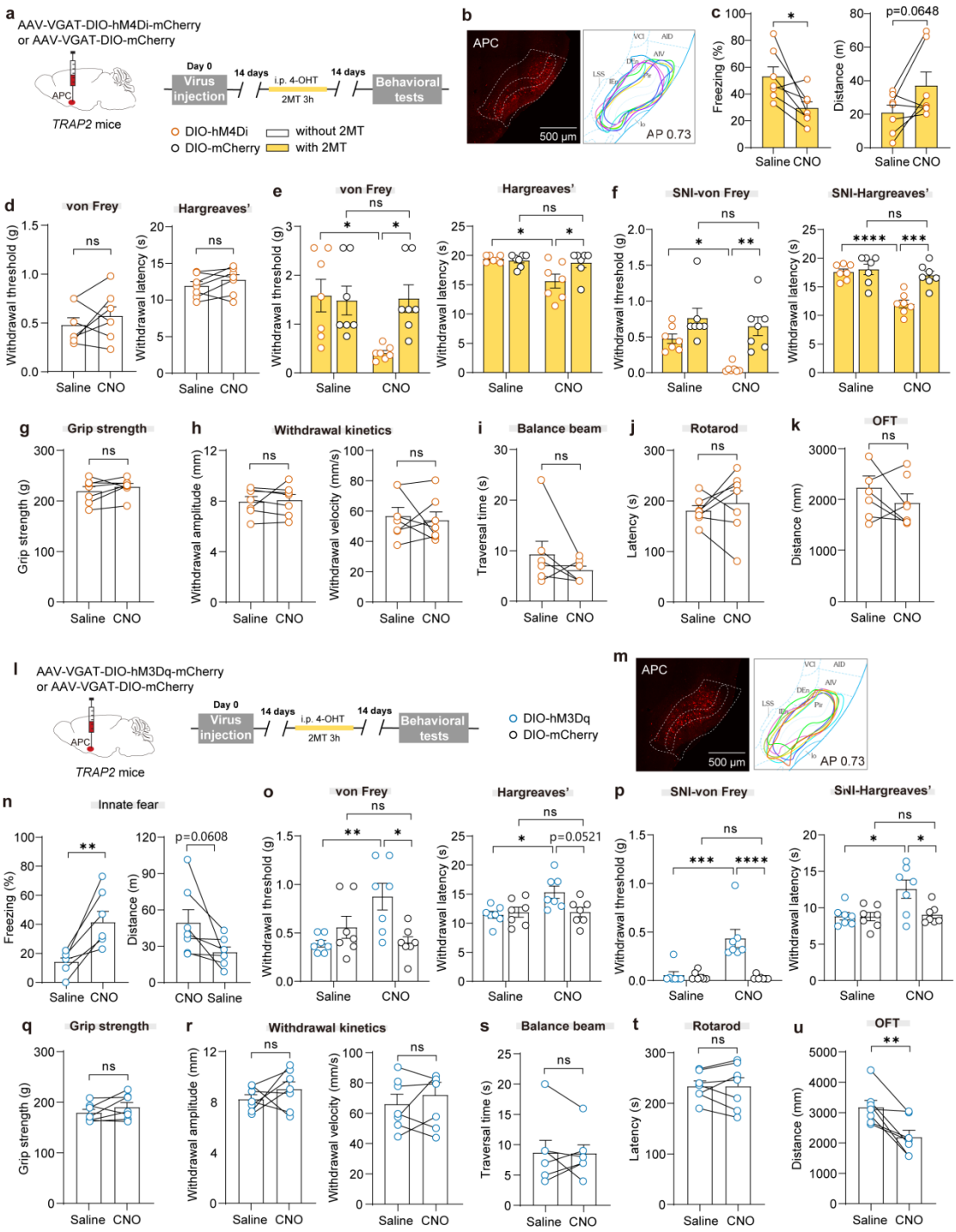

Fig 4. Chemogenetic manipulation of 2MT-activated inhibitory neurons in the APC.

a, **l**, Schematic of the viral injection and behavioral experimental timeline. **b**, **m** Left: image of coronal section showing hM4Di (**b**) or hM3Dq (**m**) expression in APC. Right: the diffusion areas of viral expression at coronal level of APC. Subjects are individually colored (n=7 mice/group). **c**,

ARTICLE IN PRESS

n, Effect of chemogenetically inhibiting (**c**: Freezing, P = 0.0257; Distance, P = 0.0648) or activating (**n**: Freezing, P = 0.0070; Distance, P = 0.0608) 2MT-TRAPed APC^{GABA} neurons on the proportion of freezing time and total moving distance (n=7 mice/group). **d**, **o**, Baseline pain sensitivity following chemogenetic inhibition (**d**) or activation (**o**: von Frey, DIO-hM3Dq&Saline vs DIO-hM3Dq&CNO, P = 0.0089; DIO-hM3Dq&CNO vs DIO-mCherry&CNO, P = 0.0112; Hargreaves', DIO-hM3Dq&Saline vs DIO-hM3Dq&CNO, P = 0.0203; DIO-hM3Dq&CNO vs DIO-mCherry&CNO, P = 0.0521) of 2MT-TRAPed APC^{GABA} neurons (n=7 mice/group). **e**, **f**, Effect of chemogenetically inhibiting 2MT-TRAPed APC^{GABA} neurons on basal nociception (**e**: von Frey, DIO-hM4Di&Saline vs DIO-hM4Di&CNO, P = 0.0259; DIO-hM4Di&CNO vs DIO-mCherry&CNO, P = 0.0384; Hargreaves', DIO-hM4Di&Saline vs DIO-hM4Di&CNO, P = 0.0103; DIO-hM4Di&CNO vs DIO-mCherry&CNO, P = 0.0449) or chronic neuropathic pain (**f**: von Frey, DIO-hM4Di& Saline vs DIO-hM4Di&CNO, P = 0.0421; DIO-hM4Di&CNO vs DIO-mCherry&CNO, P = 0.0020; Hargreaves', DIO-hM4Di&Saline vs DIO-hM4Di&CNO, P < 0.0001; DIO-hM4Di&CNO vs DIO-mCherry&CNO, P = 0.0004) of 2MT-exposed mice (n=7 mice/group). **g-k**, **q-u**, Effect of chemogenetically inhibiting (**g-k**) or activating (**q-u**) 2MT-TRAPed APC^{GABA} neurons on motor performance (n=7 mice/group, OFT, P = 0.0051). **p**, Effect of chemogenetically activating 2MT-TRAPed APC^{GABA} neurons on neuropathic pain (n=7 mice/group; von Frey, DIO-hM3Dq&Saline vs DIO-hM3Dq&CNO, P = 0.0001; DIO-hM3Dq&CNO vs DIO-mCherry&CNO, P < 0.0001; Hargreaves', DIO-hM3Dq&Saline vs DIO-hM3Dq&CNO, P = 0.0137; DIO-hM3Dq&CNO vs DIO-mCherry&CNO, P = 0.0221). Significance was assessed by two-tailed paired Student's t-test or Wilcoxon signed-rank test in (**c**, **d**, **g-k**, **n**, **q-u**), and two-way ANOVA followed by Bonferroni's multiple comparisons test in (**e**, **f**, **o**, **p**). All data are presented as the mean ± SEM. *P < 0.05, **P < 0.01, ***P < 0.001, ****P < 0.0001, not significant (ns). Details of the statistical analyses are presented in Supplementary Data 1. Source data are provided as a Source Data file.

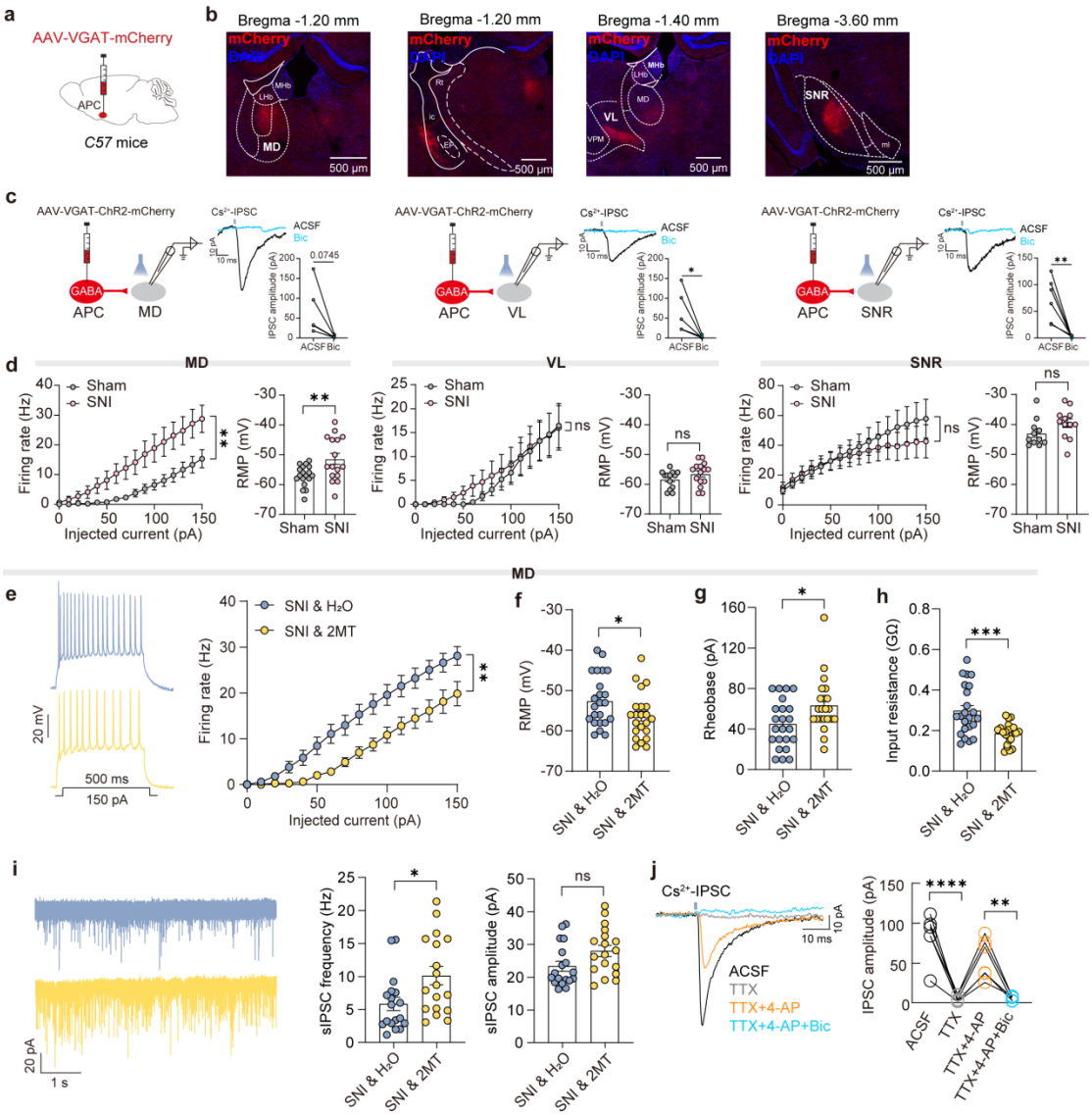

Fig 5. 2MT rescues nerve injury-induced hyperexcitability of MD neurons.

a, Schematic of viral injection into the APC of *C57* mice. **b**, Representative images showing mCherry-expressing signals in different brain regions. Scale bars, 500 μm. **c**, Schematic of MD, VL and SNR electrophysiological recordings in acute slices (left), and representative traces (right, top) and summary data (right, bottom) of blue light-evoked IPSCs before (ACSF) and after application of bicuculline (Bic, 10 μM) (n=4 mice; MD, $P = 0.0745$; VL, $P = 0.0359$; SNR, $P = 0.0096$). **d**, Summary data of firing rates and resting membrane potentials (RMP) for neurons in the MD, VL and SNR from sham control and SNI mice (MD: Sham, n=18 neurons from 4 mice; SNI, n=16 neurons from 3 mice; Firing rate, $P = 0.0093$, RMP, $P = 0.0061$. VL: Sham, n=13

ARTICLE IN PRESS

neurons from 3 mice; SNI, n=15 neurons from 3 mice. SNR: Sham, n=11 neurons from 3 mice; SNI, n=12 neurons from 4 mice). **e**-**h**, Summary data of firing rates (**e**, $P = 0.0102$), RMP (**f**, $P = 0.0379$), rheobase (**g**, $P = 0.0279$), and input resistance (**h**, $P = 0.0002$) for MD neurons from water-exposed or 2MT-exposed SNI mice (SNI & H_2O, n=23 neurons from 3 mice; SNI & 2MT, n=22 neurons from 3 mice). **i**, Representative traces and summary data of sIPSCs in MD neurons from water-exposed or 2MT-exposed SNI mice (n=18 neurons from 3 mice/group, $P = 0.0106$). **j**, Representative traces and summary data of light-evoked IPSCs in MD neurons under sequential pharmacological conditions: ACSF, TTX (1 μM), TTX and 4-AP (500 μM), and TTX & 4-AP & Bic (n=6 cells from 3 mice; ACSF vs TTX, $P < 0.0001$; TTX&4-AP vs TTX&4-AP&Bic, $P = 0.0014$). Significance was assessed by two-tailed paired Student's t-test in (**c**), two-way ANOVA followed by Bonferroni's multiple comparisons test in (**d**, firing rate; **e**), two-tailed unpaired Student's t-test or Mann-Whitney test in (**d**, RMP) and (**f**-**i**), and one-way ANOVA with Bonferroni post hoc analysis in (**j**). All data are presented as the mean ± s.e.m. *$P < 0.05$, **$P < 0.01$, ***$P < 0.001$, ****$P < 0.0001$, not significant (ns). Details of the statistical analyses are presented in Supplementary Data 1. Source data are provided as a Source Data file.

ARTICLE IN PRESS

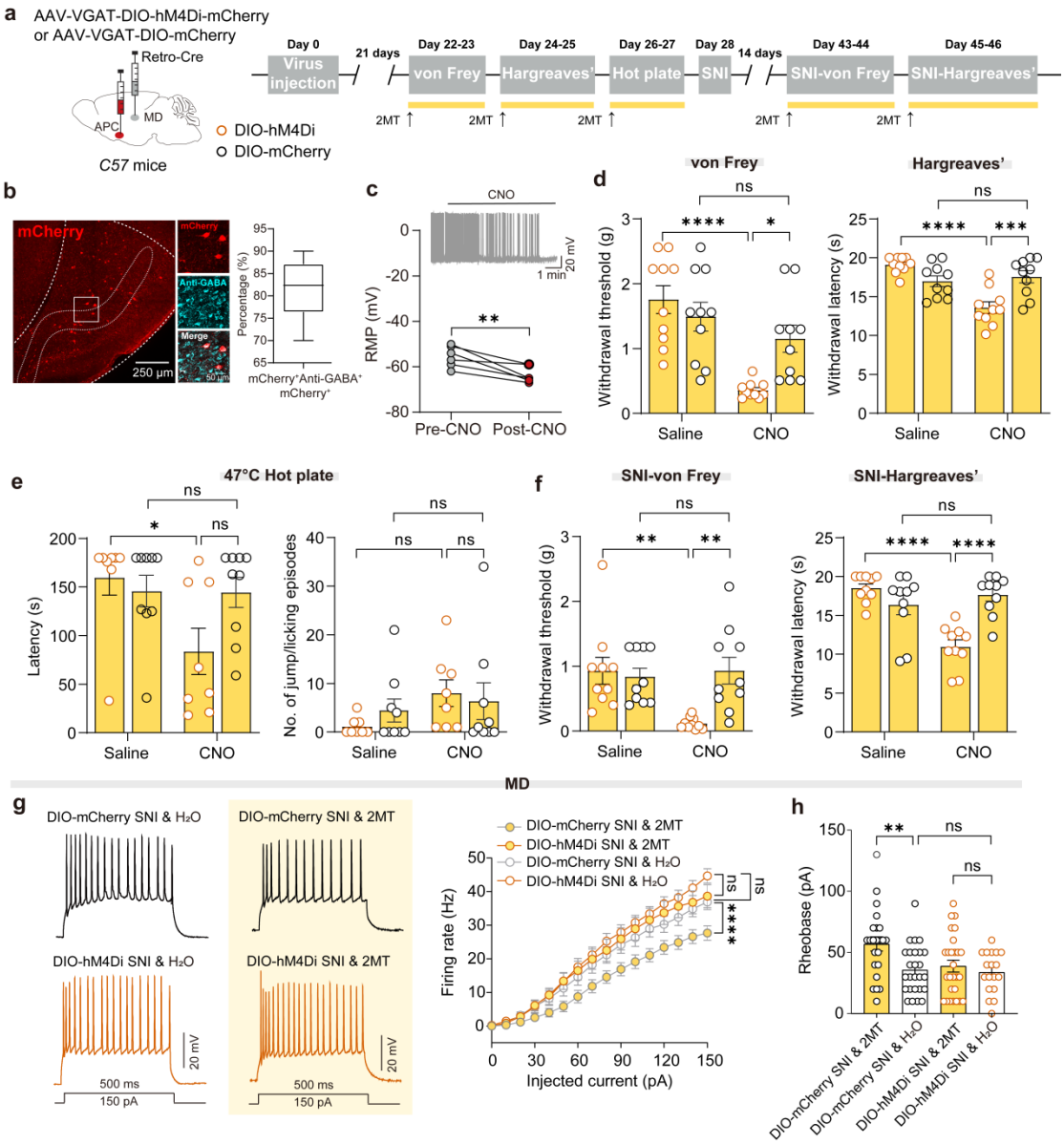

Fig 6. Inhibition of MD-projecting APC neurons attenuates 2MT-induced analgesia and 2MT-reversed MD hyperactivity in chronic pain.

a, Schematic of the viral injection and timeline of the behavioral experiments. **b**, Representative images and the percentage of mCherry-expressing neurons (red) co-localized with anti-GABA staining (cyan) in the APC (n=9 sections from 3 mice). Scale bars, 250 μm and 50 μm. **c**, Representative trace showing hyperpolarization of an hM4Di-expressing neuron after CNO application (top) and quantification of the RMP across multiple animals (bottom) (n=3 mice, P = 0.0093). **d-f**, Effects of the chemogenetic inhibition of MD-projecting APC^{GABA} neurons on the

ARTICLE IN PRESS

basal nociception (**d**: DIO-hM4Di, n=10 mice; DIO-mCherry, n=10 mice; von Frey, DIO-hM4Di&Saline vs DIO-hM4Di&CNO, $P < 0.0001$; DIO-hM4Di&CNO vs DIO-mCherry&CNO, $P = 0.0305$; Hargreaves', DIO-hM4Di&Saline vs DIO-hM4Di&CNO, $P < 0.0001$; DIO-hM4Di&CNO vs DIO-mCherry&CNO, $P = 0.0008$), acute thermal pain (**e**: DIO-hM4Di, n=8 mice; DIO-mCherry, n=9 mice; $P = 0.0499$) and chronic neuropathic pain (**f**: DIO-hM4Di, n=10 mice; DIO-mCherry, n=10 mice; von Frey, DIO-hM4Di&Saline vs DIO-hM4Di&CNO, $P = 0.0058$; DIO-hM4Di&CNO vs DIO-mCherry&CNO, $P = 0.0058$; Hargreaves', $P < 0.0001$) of 2MT-exposed mice. **g**, **h**, Effects of the chemogenetic inhibition of MD-projecting APC^{GABA} neurons on the firing rate (**g**, $P < 0.0001$) and rheobase (**h**, $P = 0.0097$) of MD neurons recorded from either water or 2MT-exposed SNI mice (DIO-hM4Di SNI&H_2O, n=18 neurons from 4 mice; DIO-mCherry SNI&H_2O, n=26 neurons from 4 mice; DIO-hM4Di SNI&2MT, n=27 neurons from 3 mice; DIO-mCherry SNI&2MT, n=23 neurons from 3 mice). Significance was assessed by two-tailed paired Student's t-test in (**c**), two-way ANOVA followed by Bonferroni's multiple comparisons test in (**d**-**g**), and one-way ANOVA followed by Bonferroni's multiple comparisons test in (**h**). All data are presented as the mean ± s.e.m except for (**b**) shown as box and whisker plots (medians, quartiles (boxes), and ranges from minimum to maximum (whiskers)). $*P < 0.05$, $**P < 0.01$, $***P < 0.001$, $****P < 0.0001$, not significant (ns). Details of the statistical analyses are presented in Supplementary Data 1. Source data are provided as a Source Data file.

ARTICLE IN PRESS

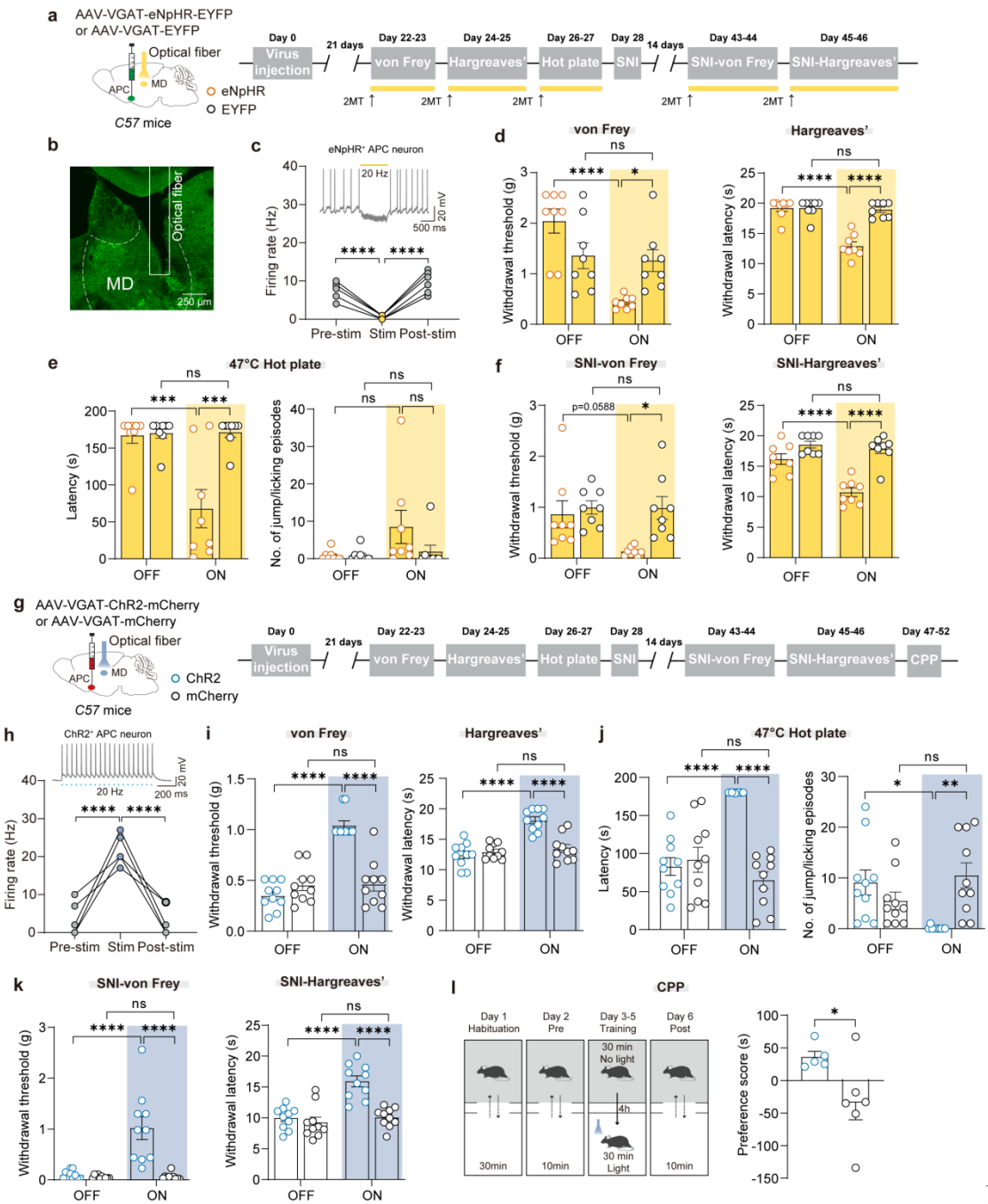

Fig 7. The APC^{GABA}-MD circuit mediates 2MT-induced analgesia.

a, **g**, Schematic of the viral injection and timeline of the behavioral experiments. **b**, Representative image of eNpHR-expressing terminals (green) and fiber implantation track in the MD. Scale bar, 250 μm. **c**, Representative trace showing blockage of the APs in an eNpHR-expressing APC neuron after yellow light illumination (594 nm, 20 Hz) (top) and quantification of the firing rates

ARTICLE IN PRESS

across multiple animals (bottom) (n=3 mice, $P < 0.0001$). **d-f**, Effects of the optogenetic inhibition of APC^{GABA} terminals within the MD on the basal nociception (**d**: von Frey, eNpHR&OFF vs eNpHR&ON, $P < 0.0001$; eNpHR&ON vs EYFP&ON, $P = 0.0487$; Hargreaves', $P < 0.0001$), acute thermal pain (**e**: Latency, eNpHR&OFF vs eNpHR&ON, $P = 0.0003$; eNpHR&ON vs EYFP&ON, $P = 0.0002$) and chronic neuropathic pain (**f**: von Frey, eNpHR&OFF vs eNpHR&ON, $P = 0.0588$; eNpHR&ON vs EYFP&ON, $P = 0.0181$; Hargreaves', $P < 0.0001$) of 2MT-exposed mice (n=8 mice/group). **h**, Representative trace showing neural firing of a ChR2-expressing neuron after blue light stimulation (473 nm, 20Hz) (top) and quantification of the firing rates across multiple animals (bottom) (n=3 mice). **i-k**, Effects of the optogenetic activation of APC^{GABA} terminals within the MD on the basal nociception (**i**: von Frey, $P < 0.0001$; Hargreaves', $P < 0.0001$), acute thermal pain (**j**: Latency, $P < 0.0001$; Episodes, ChR2&OFF vs ChR2&ON, $P = 0.0037$; ChR2&ON vs mCherry&ON, $P = 0.0151$) and chronic neuropathic pain (**k**: von Frey, $P < 0.0001$; Hargreaves', $P < 0.0001$) (ChR2, n=10 mice; mCherry, n=10 mice). **l**, Experimental schematic (left) and quantification (right) of conditioned place preference (CPP) test (ChR2, n=5 mice; mCherry, n=6 mice; $P = 0.0443$). Significance was assessed by two-way ANOVA with Bonferroni post hoc analysis in (**d-f**, **i-k**), one-way ANOVA followed by Bonferroni's multiple comparisons test in (**c**, **h**), and two-tailed unpaired Student's t-test in (**l**). All data are presented as the mean ± s.e.m. $*P < 0.05$, $**P < 0.01$, $***P < 0.001$, $****P < 0.0001$, not significant (ns). Details of the statistical analyses are presented in Supplementary Data 1. Source data are provided as a Source Data file.

ARTICLE IN PRESS

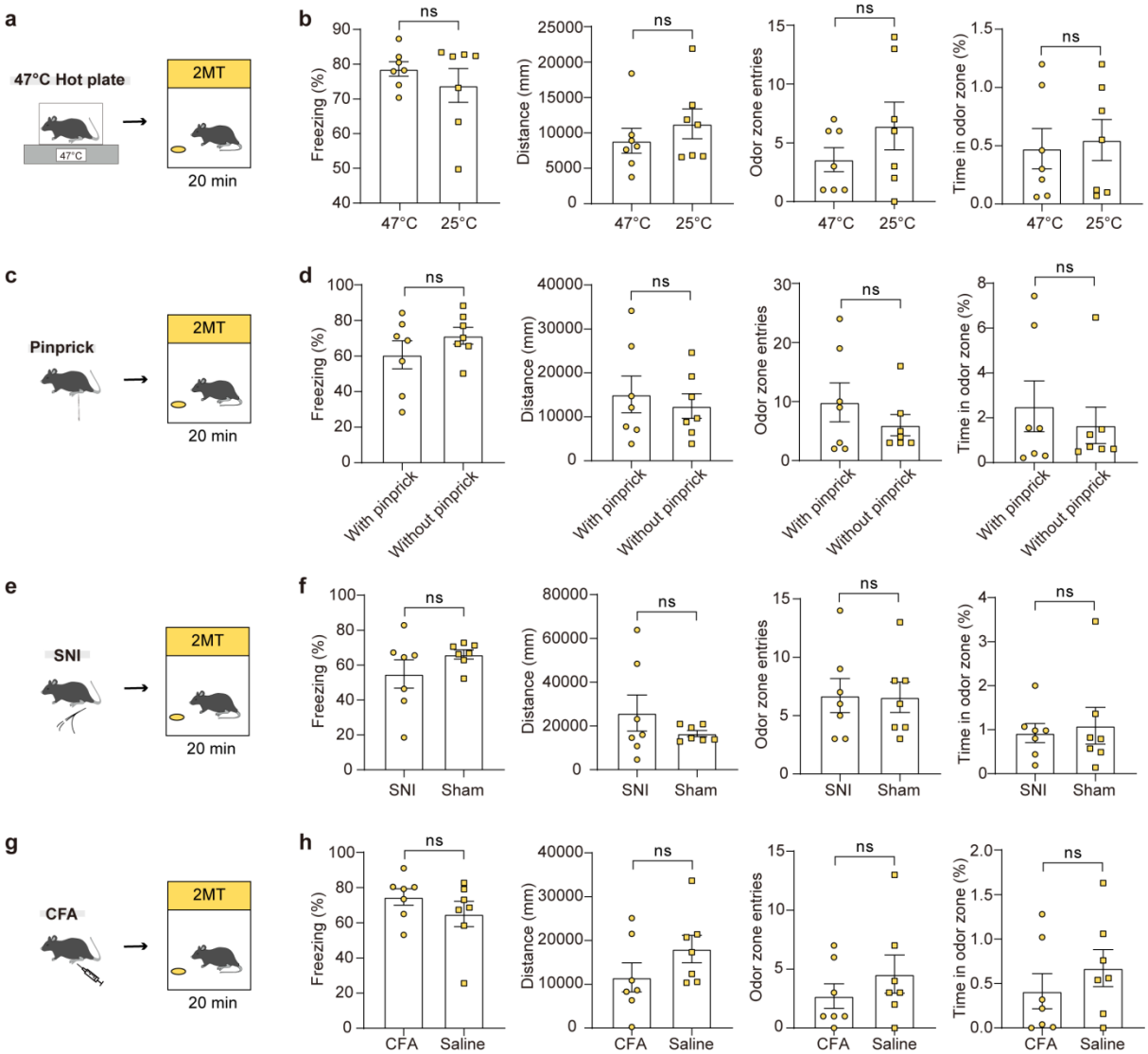

Fig 8. The innate fear responses are not affected by pain.

a, **c**, **e**, g, Experimental design for innate fear test under physiological (**a, c**) or pathological (**e**, **g**) pain conditions. **b**, Innate fear reactions assessed by the proportion of freezing time, moving distance, odor zone entries, and time in the odor zone of 2MT-exposed mice following 3-minute exposure to a 47℃ or 25℃ hot plate (n=7 mice/group). **d**, Innate fear reactions of 2MT-exposed mice following 10-trial hindpaw pinprick stimuli (n=7 mice/group). **f**, Innate fear reactions of 2MT-exposed mice with nerve injury or sham operation (n=7 mice/group). **h**, Innate fear reactions of 2MT-exposed mice with CFA or saline injection (CFA, n=7 mice; Saline, n=7 mice). Significance was assessed by two-tailed unpaired Student's t-test or Mann-Whitney U test in (**b**,

ARTICLE IN PRESS

d, **f,** **h**). All data are presented as the mean ± s.e.m. Not significant (ns). Details of the statistical analyses are presented in Supplementary Data 1. Source data are provided as a Source Data file.

ARTICLE IN PRESS

ARTICLE IN PRESS

Editor's Summary

Survival requires prioritizing threats over pain. The authors identify a brain circuit in male mice, where fear signals from the cortex block pain-associated activation in the thalamus, revealing how fear suppresses pain and offering a potential target for therapies.

Peer review information: *Nature Communications* thanks Mathieu Wolff, Nanci Winke, and the other anonymous reviewer(s) for their contribution to the peer review of this work. A peer review file is available.

ARTICLE IN PRESS